Modeling of physical and electrical properties of boron doped silicon microneedle grown by vapor liquid solid (VLS) mechanism

A thesis submitted in partial fulfillment of the requirements for the degree of

Master of Science

In

Electrical and Electronic Engineering

By

Kamrul Hasan

Under the supervision of

Dr. Md. Shofiqul Islam

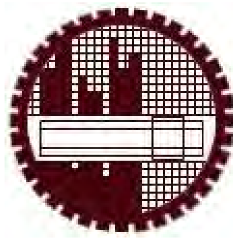

Department of Electrical and Electronic Engineering

Bangladesh University of Engineering and Technology (BUET)

July 2011

Approval

The thesis titled "**Modeling of Physical and Electrical Properties of Boron Doped Silicon Micro Needle Grown by Vapor Liquid Solid (VLS) Mechanism**" has been submitted by Kamrul Hasan, Roll no. 100706214P, Session: October 2007 to the following respected members of the Board of Examiners in partial fulfillment of the requirement for the degree of **Master of Science in Electrical and Electronic Engineering** on 25th July' 2011 and has been accepted as satisfactory.

Board of Examiners

1. __________________________ Chairman

(Dr. Md. Shofiqul Islam)
Associate Professor
Department of Electrical and Electronic Engineering
Bangladesh University of Engineering and technology (BUET), Dhaka-1000.

2. __________________________ (Ex-Officio)
(Dr. Md. Saifur Rahman)
Professor and Head
Department of Electrical and Electronic Engineering
Bangladesh University of Engineering and technology (BUET), Dhaka-1000.

3. __________________________ Member
(Dr. Md. Jahangir Alam)
Professor
Department of Electrical and Electronic Engineering
Bangladesh University of Engineering and technology (BUET), Dhaka-1000.

4. __________________________ Member
(Dr. Zahid Hasan Mahmood) (External)
Professor
Department of Applied Physics, Electronic and Communication Engineering
Dhaka University, Dhaka-1000.

Declaration

This is to certify that this thesis work is the outcome of the original work of the undersigned student. No part of this work has been submitted elsewhere partially or fully for the award of any other degree or diploma. Any material reproduced in this thesis has been properly acknowledged.

....

(Kamrul Hasan)

Roll no. 100706214P

Dedication

To all of my respected teachers

Acknowledgement

The author would like to express his sincere and profound gratitude to his supervisor Dr. Md. Shofiqul Islam, Associate Professor, Department of Electrical and Electronic Engineering, Bangladesh University of Engineering and Technology (BUET), Dhaka for his guidance, inspiration, constructive suggestions and supervision throughout the period of this thesis work. I am whole-heartedly grateful to him for his consistent guidance, encouragements, helpful suggestions and never-ending patience throughout the progress of this research work.

The author also wishes to express his gratitude to Dr. Mohammad Tarique, Assistant Professor, American International University-Bangladesh for his valuable guidance and co-operation in finding the necessary Conference and Journal papers for the thesis work.

The author is also indebted to Dr. Saifur Rahman, Professor, Department of Electrical and Electronic Engineering, BUET and to Dr. ABM Siddique Hossain, Dean, Faculty of Engineering, American International University-Bangladesh for their support and kindness.

The author would like to take this opportunity to give special thanks to the Management of American International University-Bangladesh for giving him their support and providing him printing, photocopying and internet use facilities for this thesis work.

Finally, the author would like to express everlasting gratefulness to all the family members for supporting in all situations. The author is always grateful to Almighty Allah for everything.

Abstract

Silicon microneedles are currently of great interest as one of the most useful and powerful forms of Si microstructures that could provide a promising option for emerging electronic systems. Microneedle have novel properties for various applications such as sensor, fabrication of active devices like transistors, solar cell etc. Si microneedles can be fabricated by various techniques and the Vapor-liquid-solid process (VLS) is a mechanism of forming such needle like crystal directly.

Highly conductive doped Si microneedles are required for sensing small signals and for device fabrication. By *in-situ* doping into the VLS growth method, more conductive needles can be grown. Boron-doped p-type silicon micro needles have been grown via *in-situ* doping VLS mechanism using gold (Au) as a catalyst with di-silane (Si_2H_6) as Si source and diborane (B_2H_6) as dopant source. Experimental data shows that doping changes the growth kinetics and electrical properties of the needles. Thus boron doping brings about new challenges such as control of the sizes, structures, and properties of microneedles during the synthesis step. Hence the purpose of this thesis work was to study and analyze the physical and electrical characteristics of boron doped Si-micro needles in detail with proper mathematical modeling.

At first, the effect of doping level on the growth rate of the microneedle was analyzed. A mathematical model relating growth rate with doping level was derived which is compatible with the experimental result. Similarly the effect of microneedle diameter on the growth rate has been explained with mathematical relation based on the experimental data and related research works. Again the dependency of the diameter of the needle on doping level and other initial conditions of VLS growth was analyzed and explained in this work. At last the electrical characteristics of the boron doped Si microneedle was investigated and explained using the physics of metal-semiconductor junction, Schottky barrier and band theory. All the results of this work have been compared with experimental data to justify the compatibility of the models.

The mathematical model and analysis in this thesis will be very helpful to anticipate the size of such Boron doped microneedles and hence to fabricate microneedles of desired length and width for certain applications. The analysis of the electrical properties work will also be helpful to improve the J-V characteristics in future while fabricating vertical devices like diodes, transistors with Si microneedles.

Table of Contents

APPROVAL ..... **II**

DECLARATION ..... **III**

DEDICATION ..... **IV**

ACKNOWLEDGEMENT ..... **V**

ABSTRACT ..... **VI**

LIST OF ABBREVIATIONS ..... **IX**

LIST OF TABLES ..... **X**

LISTS OF FIGURES ..... **XI**

1. CHAPTER 1 (INTRODUCTION) **2**

1.1 SCOPE OF THE THESIS 2
1.2 STATE OF THE PROBLEM 3
1.3 APPLICATIONS OF MICRONEEDLES 4
1.3.1 Biotechnology *4*
1.3.2 Medical science *5*
1.3.3 On-chip devices *5*
1.3.4 Force and Temperature sensing *6*
1.4 REVIEW OF PREVIOUS WORK 6
1.5 OBJECTIVE 8
1.6 APPROACH 8
1.7 ORGANIZATION OF THIS THESIS 9

2. CHAPTER 2(MICRONEEDLE FABRICATION) **12**

2.1 FABRICATION PROCESS 12
2.2 VLS MECHANISM 13
2.2.1 Introduction *13*
2.2.2 Fundamentals of VLS mechanism *13*
2.2.3 VLS Growth Process *14*
2.2.3.1 Alloying process 14
2.2.3.2 Nucleation process 15

2.2.3.3 Axial growth 15
2.3 *In Situ* doped VLS 16
2.3.1 p-Si Microneedle Fabrication 16
2.3.2 Results 18

3. CHAPTER 3(GROWTH RATE ANALYSIS) 21

3.1 Introduction 21
3.2 Effect of Boron Doping on microneedle growth rate 22
3.2.1 Experimental Findings 22
3.2.2 Theoretical Analysis 23
3.2.2.1 Sticking Property of Boron 24
3.2.2.2 Loss of Au during VLS growth. 24
3.2.3 Mathematical Modelling 25
3.3 Effect of droplet size on microneedle growth rate 28
3.3.1 Experimental Findings 28
3.3.2.1 Fundamentals of Crystal Growth 30
3.3.2.2 Gibbs-Thomson Effect 31
3.3.2.3 Diffusion Effect 32
3.3.3 Combining the Gibbs-Thomson effect and Diffusion effect 34

4. CHAPTER 4(DIAMETER ANALYSIS) 40

4.1 Introduction 40
4.2 Effect of Au dot size on microneedle diameter 40
4.2.1 Experimental Findings 41
4.2.2 Theoretical Analysis 43
4.2.3 Mathematical Relation 43
4.3 Effect of doping on microneedle diameter 45
4.3.1 Experimental Findings 45
4.3.2 Theoretical Analysis 47

5. CHAPTER 5(METAL-SEMICODUCTOR JUNCTION THEORY) 51

5.1 Introduction 51
5.2 Metal-Semiconductor Junction 52
5.3 Ideal case of Barrier height 54
5.4 Junction Under Biasing 55
5.5 Current Transport Method 56
5.6 Thermionic emission theory 57

6. CHAPTER 6(I-V CHARACTERISTIC ANALYSIS) 62

6.1 INTRODUCTION 62
6.2 EXPERIMENTAL FINDINGS 62
6.3 J-V ANALYSIS 64
6.3.1 metal-p-type semiconductor contact 64
6.3.2 Simulation Result 66
6.3.3 J-V Equation 67
6.3.4 Comparison between Experimental and Simulation Result 68
6.5 REASONS FOR DEVIATIONS FROM THE IDEAL CASE 70
6.5.1. Schottky Barrier Lowering 71
6.5.2. Surface Imperfections 71
6.5.3. Tunneling 71
6.5.4. Series Resistance 71
6.5.5 Edge Effects 71

7. CHAPTER 7(CONCLUSION AND FUTURE WORK) 73

7.1 CONCLUSION 73
7.2 SCOPE OF FUTURE RESEARCH WORK: 74

REFERENCES 76

List of Abbreviations

CVD	**Chemical Vapor Diposition**
FET	**Field Effect Transistor**

GS-MBE **Gas-Source Molecular-Bean-Epitaxy**

MEMS **Micro Electro Mechanical System**

SEM **Scanning Electron Micrographs**

VLS **Vapor Liquid Solid**

List of Tables

Table 2.1: Experimental data of microneedle growth 19

Table 3.1: Growth rate variation of P-Si microneedle from experimental data with various doping level of P-Si microneedle at a temperature of 700^0C and at the growth pressure of 5×10^{-3} Pa. 22

Table 3.2: Growth rate variation of P-Si microneedle from experimental data and from the model. 27

Table 3.3: Growth rate for different Au dot size. 29

Table 4.1: Microneedle diameter for different Au dot size. 43

Table 4.2: Experimental data for microneedle diameter for different doping level. 46

Table 6.1 : J-V characteristics Data of p-Si microneedle with a length of 38.57 µm and a diameter of 3.30 µm for a B_2H_6 flow rate of 1.57 sccm. 63

Table 6.2: Table comparing Experimental and Simulated data for J-V characteristic... 69

Lists of Figures

Figure 1.1 : Microneedle electrode grown by dry etching inserted into cells for intracellular recording [1] 4

Figure 1.2 : Schematics of a conventional p-channel MOSFET and a silicon nanowire vertical surround-gate field-effect transistor grown by VLS method.[6] 5

Figure 1.3: Out-of-plane silicon microwire-based artificial whisker array sensor by selective VLS growth of p-silicon on an n-silicon [7] 6

Figure 1.4 : Needle grown on Si substrate by VLS method. 7

Figure 2.1 : Various MEMS basic processes.. 1

Figure 2.2 : Three basic stages of VLS mechanism. 13

Figure 2.3 : Binary Au-Si phase diagram 15

Figure 2.4 : Micro needles grown by vapor-liquid-solid mechanism 16

Figure 2.5 : Fabrication steps of p-Si microneedle by VLS growth. 17

Figure 2.6: SEM image of a typical (7x6) array of p-Si microneedle array grown by *in situ* doped VLS at 690^0C at the growth pressure of 5×10^{-3} Pa using the ratio of B_2H_6 to Si_2H_6 of 6882 ppm for 90 min. [13]. 18

Figure 3.1 : Growth rate variation with doping level of P-Si microneedle grown by VLS at temperature around 700^0C. 23

Figure 3.2 : Two effects of boron doping on the growth rate of boron doped Si microneedle. 23

Figure 3.3 : (a) Bright-field TEM images of the undoped-doped transition area of the same nanowire. (b) High-resolution image of the transition area of the nanowire where the darker contrast areas are the Au rich reason. [13] 1

Figure 3.4: Growth rate variation of p-Si microneedle as a function of doping, grown by VLS at a temperature of 690^0C and at the growth pressure of 5×10^{-3} Pa. 27

Figure 3.5 : Growth rate (µm/min) Vs Au dot size (µm) for various B_2H_6 Flow rate. .. 29

Figure 3.6 : Scanning electron micrographs of GaP nanowires grown with MOVPE at different temperatures: (A) 440 °C, (B) 470 °C, and (C) 500°C [25]. 32

Figure 3.7: Contribution of diffusion in needle growth 33

Figure 3.8: experimentally grown boron doped Si microneedle 34

Figure 3.9 : Top: Scanning electron micrographs indicating the development of the droplet shape in the initial phase of growth [26]. Center: Schematic development of droplet and wire shape in the initial phase of growth.. Bottom: the corresponding equilibrium balance of surface forces at the left edge of the droplet (dashed circles). .. 35

Figure 3.10: (a) Au-si alloy droplet on Si microneedle ($\beta>90^0$) (b) spherical coordinate system. 36

Figure 4.1: Experimental results on Microneedle diameter as a function of Au dot size for B_2H_6 flow rate (a) 0.12 sccm (b) 0.39 sccm 42

Figure 4.2 : Theoretical relation between Microneedle diameter and Au dot diameter. 45

Figure 4.3: Microneedle diameter Vs doping level. 46

Figure 4.4 : Contact angle (measured in the gas phase) as a function of temperature.[18] 47

Figure 4.5: Vectorial equilibrium for a droplet of a liquid resting on a solid. 48

Figure 5.1: Band diagram of metal and n-type semiconductor before contact 53

Figure 5.2: Band diagram of metal and n-type semiconductor after contact 53

Figure 5.3: Electronic energy relations of a high work-function metal and an n-type semiconductor.. 54

Figure 5.4: Energy-band diagrams of metal on n-type (left) and on p-type (right) semiconductors under different biasing conditions. (a) Thermal equilibrium. (b) Forward bias. (c) Reverse bias.[30]... 55

Figure 5.5:Five fundamental transport processes under forward bias. (1) Thermionic emission. (2) Tunneling. (3) Recombination. (4) Diffusion of electrons. (5) Diffusion of holes.[30]. 56

Figure6.1: J-V characteristics curve of p-Si microneedle with a length of 38.57 µm and a diameter of 3.30 µm for a B_2H_6 flow rate of 1.57 sccm. 63

Figure 6.2: SEM image of p-Si microneedle array grown by *in situ* doped VLS [13]. . 64

Figure 6.3: Band diagram of Metal-p-Si junction under biased condition. 65

Figure 6.4 : J-V characteristics curve of p-Si microneedle from the Atlas simulator. ... 66

Figure 6.5 : J-V Comparison between the simulated and experimental data 69

Figure 6.6: Effect of changing work function on J-V characteristics............................. 70

Figure 7.1: Increase in the number of publications on nanowire related topics from year 1991-2009 (Source, ISI; keyword, nanowires)... 73

CHAPTER 1

Introduction

Chapter 1

Introduction

1.1 Scope of the thesis

The rising demand of low-dimensional Si microstructures for various applications (MEMS application) has attracted the attention of the researchers towards the fabrication of Si micro needles. These Si micro needles can be used in many applications such as inserting needle for sensing signals for biomedical applications [1]-[5], for the fabrication of vertical active devices like diodes and transistors [4]-[6] microneedle array sensor for both force and temperature detection [7]. Si micro needles can be fabricated by various ways like chemical vapor deposition (CVD) method, etching technique etc but the Vapor-liquid-solid process (VLS) [5] is a mechanism of forming such needle like crystal directly.

However the importance of these microneedles as sensors and for other applications has motivated this thesis work. For the successful utilization and growth of these microneedles, proper modeling and characterization of both physical and electrical properties is must. Literature shows that most of the previous researchers reported intrinsic type Si micro needles grown by VLS using only Si gas source. The main goal of this research work is the modeling and detail analysis of physical and electrical properties of boron doped silicon micro needle grown by vapor liquid solid (VLS) mechanism.

1.2 State of the problem

Intrinsic type Si micro needles grown by VLS using only Si gas source are not suitable for some applications such as its high resistivity (~ $10^4\Omega$) is a barrier for collecting small valued neural signal and again undoped Si is not suitable for device fabrication; therefore, highly conductive doped needles were demanded. The conventional thermal doping at 1100^0C can improve conductivity but this high temperature is detrimental to on-chip devices [9]. Conversely lower is unable to dope the probes sufficiently; it was observed that at 900ºC the depth of doping was 0.5 μm from the surface of the needle sidewall [10]. Thus temperature issue was a great barrier to fabricate highly conductive probes with on-chip circuitry by conventional way of thermal diffusion. However, introducing *in-situ* doping into the VLS growth method, more conductive probes can be grown at a lower temperature around 700°C [11]. Boron-doped p-type silicon micro needles have been grown via *in-situ* doping VLS mechanism using gold (Au) as a catalyst with di-silane (Si_2H_6) as Si source and diborane (B_2H_6) as dopant source [11].

Experimental data shows that mixing of diborane with disilane changes the growth kinetics and electrical properties of the needles. It was observed by the researchers that boron doping changes the growth characteristics of the microneedles significantly if compared with the intrinsic one. The growth rate first increases with the increment of boron doping and after certain level of boron incorporation the growth rate decreases. The reason behind this mysterious behavior was unanswered and this research work has given a light to the mystery with successful analysis and modeling [12]. Again boron doping also changes the electrical characteristics. Conductor like linear I-V characteristics was expected but experimental results show different nature. The I-V characteristic was found to be linear in one direction and rectifying in the opposite direction. This rectifying behavior was also hazy to the researchers. A complete analysis and model of this rectifying behavior of boron doped Si microneedles is also proposed in this work.

1.3 Applications of microneedles

Microneedles has a huge prospect as MEMS (Micro-Electro-Mechanical Systems) which means miniaturized mechanical and electro-mechanical elements that are made using the techniques of micro fabrication. There are various applications for MEMS in the field of biotechnology, medicine, communication and internal sensing. This modern technology has contributed a lot in the field of biology and microelectronics. Recently researchers are exploring the field of nanotechnology to a great extent but mechanically robust structure is required during penetration into tissues such as the brain, peripheral nerves, etc. the microstructure is mechanically strong and hence suitable for certain applications especially as sensors. Microneedle has a huge prospect to use as a sensing due to their special needle like shape and mechanical strength [7]. Here are a few applications of microneedles:

1.3.1 Biotechnology

The living cell response to an external electrical field is a fundamental method for drug development and disease studies. Microneedle can be used in such biomedical application as sensor for their special needle like shape. At present various MEMS are used for DNA amplification and identification, biochips for detection of hazardous chemical and biological agents, and for high-throughput drug screening and selection. J. Held et al [1] has reported the use of microneedle for the electroporation of adherently growing cells and intracellular recording with focus on the influence on external factors on the cell behavior. The figure below shows how they used microneedles for intra cellular recording.

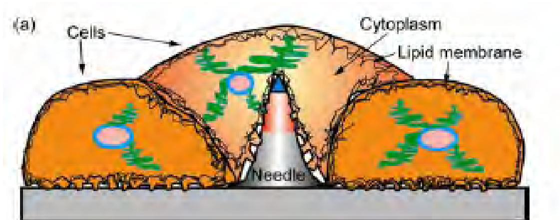

Figure 1.1 : Microneedle electrode grown by dry etching inserted into cells for intracellular recording [1]

1.3.2 Medical science

Applications for MEMS in medicine are numerous. The most successful application of MEMS in medicine is as pressure sensors, some of the applications of MEMS pressure sensors in medicine include blood pressure and respiration monitoring system, barometric pressure sensing, in kidney dialysis monitoring system and drug delivery etc. The contribution to patient care for all of these applications has been enormous. It is obvious that MEMS has already contributed a lot in the field of medical science. At present MEMS electrodes are also being used in neuro-signal detection and neuro-stimulation applications. T. Kawano et al have reported on the development of neural recording chip device with penetrating Si microprobe electrode array using IC-process [3]. These microneedles also have prospective applications in the chemical and biomedical fields for localized chemical analysis and programmable drug-delivery systems [5].

1.3.3 On-chip devices

K. Takei et al have reported the fabrication of Si microprobes and on-chip NMOSFETS and also tested the electrical characteristics as well as the mechanical feasibility of the needles to insert into neural network of human brain in order to collect neural signal [4]. Realization of Si vertical surround gate FET (Fig 1.2) is reported by V. Schmidt et al [6]. This kind of vertical surround gate can also be fabricated in micro scale which will be suitable to use as sensors for their mechanical robustness.

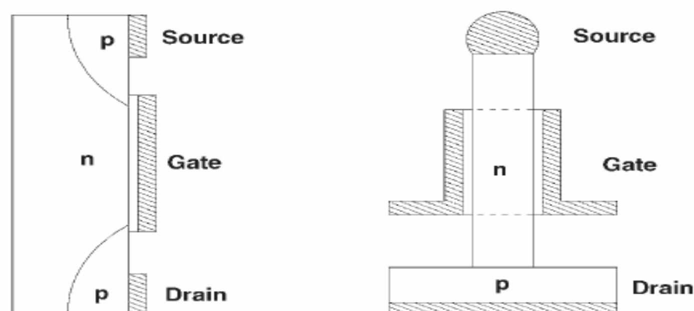

Figure 1.2 : Schematics of a conventional p-channel MOSFET and a silicon nanowire vertical surround-gate field-effect transistor grown by VLS method.[6]

1.3.4 Force and Temperature sensing

Recently A. Ikedo et al have proposed an out-of-plane high-aspect-ratio microneedle array sensor which can be used for both force and temperature detection utilizing the piezoresistance effect of semiconducting materials [7]. The figure below shows the method.

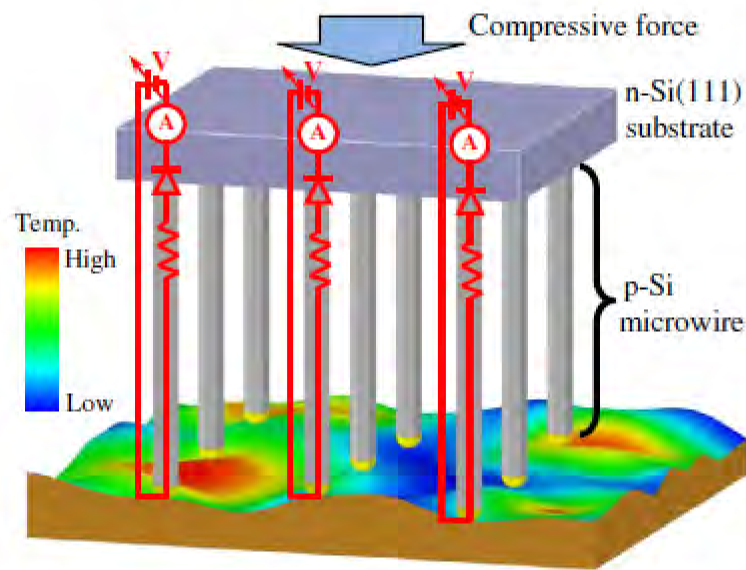

Figure 1.3: Out-of-plane silicon microwire-based artificial whisker array sensor by selective VLS growth of p-silicon on an n-silicon [7]

1.4 Review of previous work

The Vapor Liquid Solid (VLS) mechanism was first reported by Wagner in1964 as a method for silicon whisker growth [7]. The vapor-liquid-solid process (VLS) is a mechanism of forming needle-like crystal directly. In this method the dots of a metallic catalyst (normally Au) are formed on Si substrate. Then the substrate with Au dots is heated in a vacuum chamber and then Au-Si liquid alloy droplets are formed on the Si surface as Au mix with Si atoms of the substrate. Now if the gas source of Si is introduced into the chamber, Si atoms from the gas are absorbed by the Au-Si liquid alloy droplet. When the droplet becomes supersaturated, Si atoms begin to precipitate at the interface of alloy droplet and substrate and hence needle-like Si crystal grows

perpendicular to Si surface as shown in Fig 1.3. The VLS method is discussed in detail in Chapter 2 of this work.

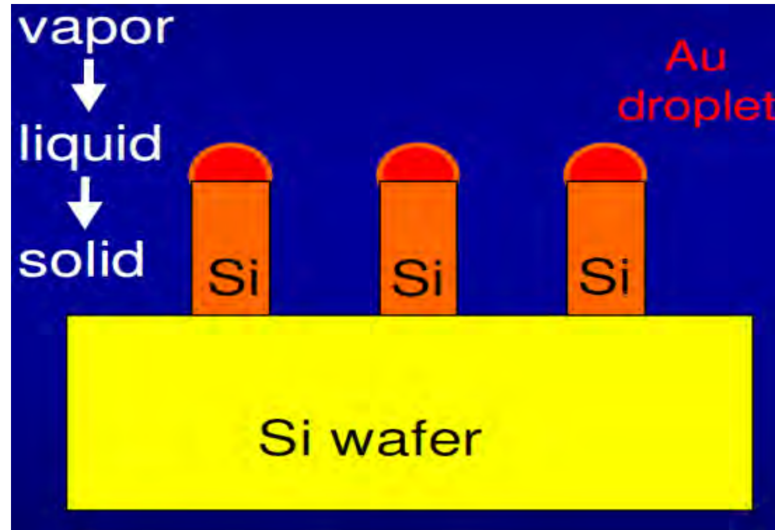

Figure 1.4 : Needle grown on Si substrate by VLS method.

However Since 1964 researchers are using this method as an effective way of fabricating needle like structures both in micro and nano scale for various applications [1]-[6]. But most of the previous researchers reported about intrinsic type microneedle and the main problem of these intrinsic type needles is the high resistivity which is an obstacle towards collecting small signals. A group of researchers, M.S Islam et al in the Toyohashi University of Technology; Japan introduced an alternate approach by incorporating *in situ* doping into VLS growth system and thus they obtained doped Si microprobes at low temperature (around 700ºC) [11]-[13]. This method of *in situ* doping solved the temperature and resistivity issues as described in section 1.2 to a great extent. Both P-type and N-type microneedles were grown successfully by the group. Experimental data was collected and reported where some deviation in growth and electrical characteristic was found in case of boron doped P-Si microneedles. This research work has covered the complete growth and electrical analysis with mathematical modeling.

1.5 Objective

This work has the following objectives related to boron doped silicon microneedle formed by *in situ* VLS method:

i) To model the growth rate of boron doped silicon microneedle as a function of Au dot size and doping level.

ii) Modeling of the diameter of the needle as a function of the Au dot size and doping level.

iii) Analysis of the current-voltage (I-V) characteristics of boron doped silicon microneedle.

The results of this work will be necessary to predict the length, diameter and electrical properties of the needle required for certain application.

1.6 Approach

The growth rate of boron doped silicon micro needle is influenced by various factors like the properties of the liquid alloy, the gas flow rate, Au dot size, doping level, the ambient temperature and pressure etc [14]- [16]. At first this work has analyzed the effect of changing doping level on the growth rate for a fixed Au dot size. From previous reports it was found that boron doping enhances the gas absorption rate and causes some loss of Au in the needle simultaneously [14]. This loss of Au reduces the Au droplet size on the top of the needle. The interaction of these two phenomena has been investigated and a mathematical model expressing the relationship between the growth rates and doping level has been developed [12]. Solid defects caused by gold in Si needle [14] , sticking properties of boron, gas phase reaction of disilane (Si_2H_6) and diborane (B_2H_6) [16] has been considered carefully for the modeling. Similarly for a

constant doping level the growth rate variation of boron doped Si microneedles has been investigated as a function of Au dot size.

Again the diameter of the needle depends on Au-Si liquid alloy droplet size, which is directly related to the Au dot size. However, the size of the droplet is affected by the viscosity and surface tension of liquid Au-Si alloy as well as the wetting of Si by liquid Au-Si alloy [17]-[20]. All these factors are considered for the modeling of the needle diameter as a function of Au dot size. Similarly the effect of doping on the diameter has been analyzed.

Experimental result exhibits nonlinear I-V relationship whereas, a simple doped needle is expected to provide linear I-V characteristics. This nonlinearity indicates the probability of having any rectifying junction specifically on top of the needle where some Au-Si alloy remains after needle formation. Related physics of metal-semiconductor junction, Fermi level, Schottky barrier and band theory [21], electron transport process [22] has been used to analyze the I-V characteristics and also the experimental result is compared with the simulation.

1.7 Organization of this thesis

This thesis consists of six chapters. Chapter-1 is concentrated on the purpose and scope of the work, back ground and present state of the problem, objective and methodology.

In chapter-2, a brief overview of the different methods of microneedles fabrication, the VLS mechanism and the experimental procedure of microneedles growing process is covered.

In chapter-3, the growth rate of boron doped Si microneedle is analyzed and mathematical model is designed.

Chapter-4 includes the modeling of the needle diameter as a function of Au dot size. Similarly the effect of doping on the diameter has been analyzed in this chapter.

Chapter-5 contains a theoretical overview of metal-semiconductor junction and basic current transport processes through the contact. The thermionic emission theory of current transport is discussed in detail and derivation of J-V equation also included in the chapter.

In chapter-6, the electrical properties of boron doped Si microneedle are analyzed and the J-V characteristics are compared with simulation.

Finally, conclusions and some proposals for future work are given in chapter-7.

CHAPTER 2

Microneedle Fabrication

Chapter 2

Microneedle Fabrication

2.1 Fabrication Process

The technology of driving very small mechanical devices by electricity is known as MEMS. It merges at the nano-scale into NEMS (Nanoelectromechanical systems) and nanotechnology. Usually MEMS are supposed to be between 1 to 100 micrometres in size (i.e. 0.001 to 0.1 mm). With the advancement of semiconductor device fabrication technologies, normally used to make electronics, MEMS became practical as the fabrication became feasible. MEMS technology can be implemented by different materials and manufacturing techniques. These include patterning, wet etching and dry etching, electro discharge machining (EDM), CVD and VLS and other technologies capable of manufacturing small devices. Fig 2.1 shows MEMS basic processes.

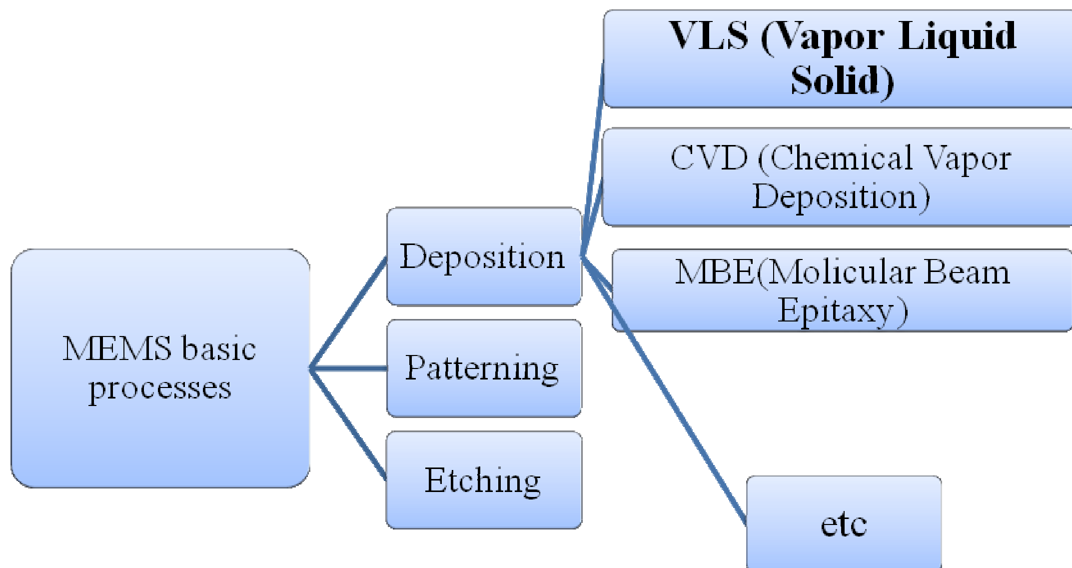

Figure 2.1 : Various MEMS basic processes.

2.2 VLS Mechanism

2.2.1 Introduction

First introduced by Wagner in 1964[7] the vapor-liquid-solid process (VLS) is a mechanism for the growth of needle like structures like microneedles and nanowires. Similar structures can also be grown from chemical vapor deposition (CVD). In CVD method crystal growth is through direct adsorption of a gas phase on to a solid surface which is generally very slow. The VLS mechanism overcome this by introducing a catalytic liquid alloy phase which works like a trap and can rapidly adsorb the atoms of constituents from vapor to supersaturation levels. Thus crystal growth occurs from the nucleation of seeds at the liquid-solid interface. The VLS mechanism can be described in three stages as in the figure below.

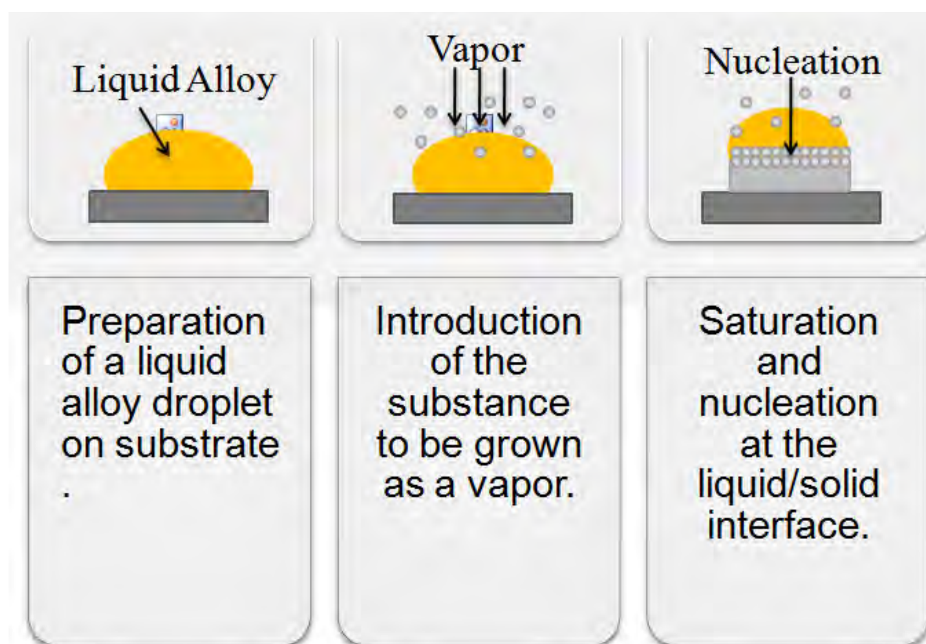

Figure 2.2 : Three basic stages of VLS mechanism.

2.2.2 Fundamentals of VLS mechanism

Wagner summarized the experimental details, results and VLS theory in a truly elegant way which was further elaborated by Givargizov who developed the experimental observations and models and theories regarding the VLS process. In the

recent years, extensive research in this field has been carried out but the fundamental of the VLS method have not changed much. Wagner summarized the requirements for the VLS growth as bellows:

- The catalyst or impurity must form a liquid solution with the crystalline material to be grown at the deposition temperature.
- The distribution coefficient of the catalyst or impurity must be less than unity at the deposition temperature.
- The equilibrium vapor pressure of the catalyst or impurity over the liquid droplet must be very small. Although the evaporation of the catalyst does not change the composition of the standard liquid composition, it does require the total volume of the liquid droplet. Unless more catalyst is supplied, the volume of the liquid droplet reduces.
- The catalyst or impurity must be inert chemically. It must not react with the chemical species such as by-products present in the growth chamber.
- The interfacial energy plays a very important role. The wetting characteristic influences the diameter of the probes. For a given volume of liquid droplet, a small wetting angle results in a large growth area, leading to a large diameter.
- For a compound growth, one of the constituents can serve as the catalyst.
- For controlled unidirectional growth, the solid-liquid interface must be well defined crystallographically. One of the simplest methods is to choose a single crystal substrate with desired crystal orientation.

2.2.3 VLS Growth Process

In order to illustrate the process of the VLS growth the growth of silicon microneedles with gold as a catalyst and Si as substrate is taken as an example.

2.2.3.1 Alloying process

At first a thin layer of gold is deposited on silicon substrate and annealed at an elevated temperature (above the eutectic point of 380^0C of the silicon-gold system), which is typically same as the growth temperature. During the annealing, silicon and gold react and form a liquid mixture, which forms a droplet on the silicon substrate

surface. During the growth, an equilibrium composition is reached at the growth temperature as determined by the binary phase diagram as shown in Fig. 2.3.

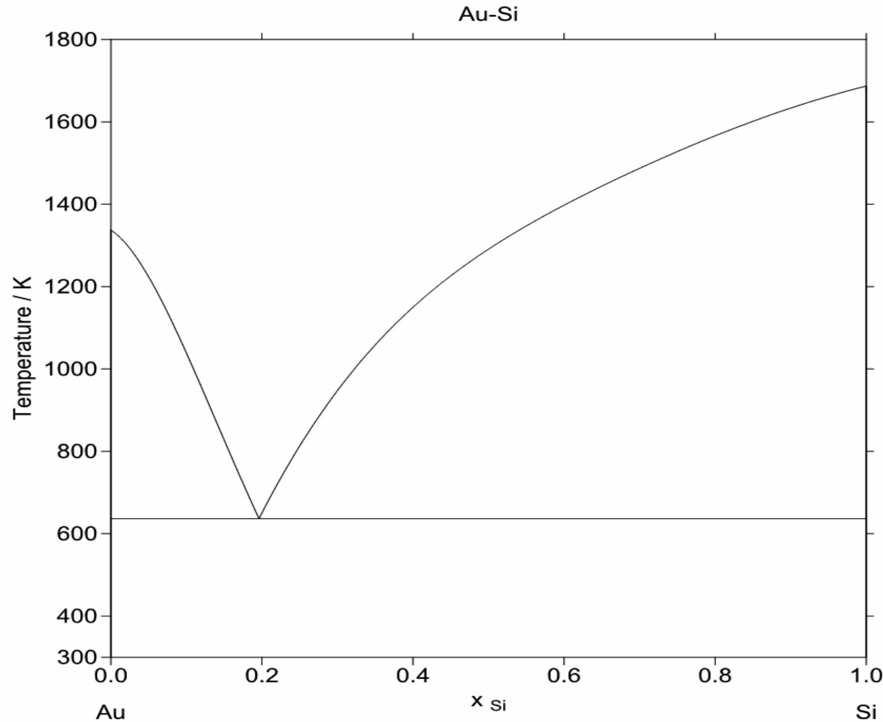

Figure 2.3 : Binary Au-Si phase diagram

2.2.3.2 Nucleation process

When Si vapor is introduced from the source the droplet acts like a trap and the gas preferably condensed at the surface of the liquid droplet. Thus the liquid droplet become supersaturated with silicon atoms which ultimately diffuse from the liquid-vapor interface and precipitate at the solid-liquid interface.

2.2.3.3 Axial growth

Once the Si crystal nucleates at the liquid/solid interface the axial growth starts. Further condensation of Si vapor into the system increases the amount of precipitation. The incoming Si species prefer to condense at the existing solid/liquid interface as this

requires less energy involvement. Thus the growth proceeds perpendicularly to the solid-liquid interface and ultimately needles grow as in the following figure.

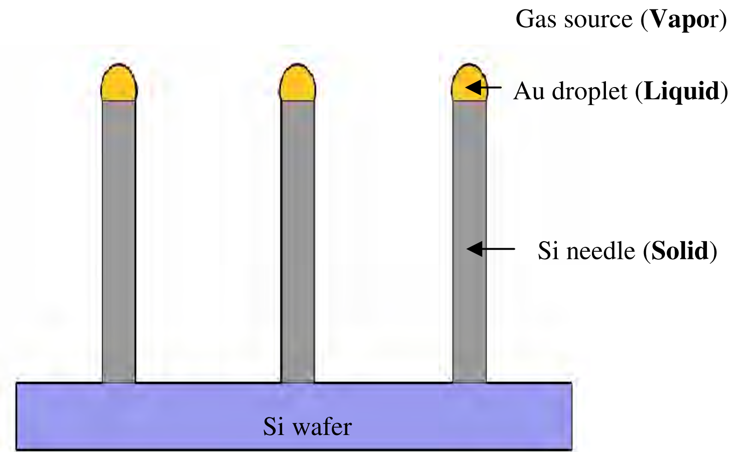

Figure 2.4 : Micro needles grown by vapor-liquid-solid mechanism

2.3 *In Situ* doped VLS

Incorporating *in situ* doping into VLS growth system doped Si microneedles can be grown at low temperature (around 700º) [13]. In this method, doping materials is introduced as vapor during the VLS growth and thus the needles are doped. The doping concentration is controlled by changing the flow rate of the doping species. A group of researchers, in the Toyohashi University of Technology; Japan grew boron doped p-type Si microneedles by incorporating *in situ* doping into VLS growth system at low temperature (around 700ºC) [11]-[13].The result of the experiment is used in this work for analysis.

2.3.1 p-Si Microneedle Fabrication

In the experiment p-Si (111) wafer was used as a substrate. Fig .2.5 shows the steps of fabrication of p-Si microneedle by VLS. First of all using wet oxidation at 1100^0C, about 900 nm thick SiO_2 layer was formed on p-Si (111) substrate (Fig. 2.5a). Then arrays of circular windows through SiO_2 was created by photolithography and

SiO_2 etching with buffered hydrofluoric acid (BHF) as shown in Fig. 2.5b. Then 50-200nm thin film of Au was deposited over the pattern by evaporation technique. (Fig. 2.5c).Then by lift-off process the Au film was removed from the resist-surface and thus Au dots of desired diameter remained in the arrays of circular SiO_2 windows as in Fig. 2.5d since surface was exposed through these windows.

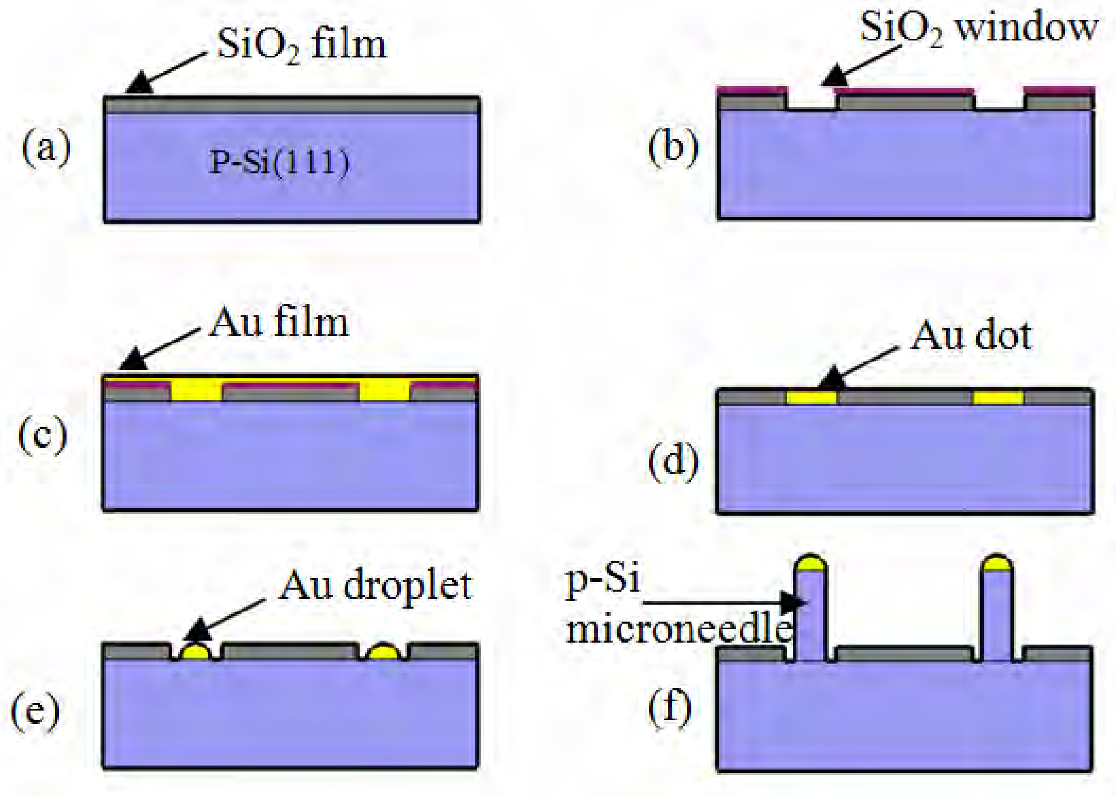

Figure 2.5 : Fabrication steps of p-Si microneedle by VLS growth.

Then the sample with Au dots was inserted into a high-vacuum gas-source molecular-bean-epitaxy (GS-MBE) chamber. The chamber was equipped with 100% Si_2H_6 as Si source and 1% B_2H_6 (diluted in 99%H_2) to assist *in-situ* doping of the needles grown by VLS mechanism. It was possible to control the boron-to-silicon ratio in the inlet gas system by adjusting the flow rate of B_2H_6 and Si_2H_6. At a temperature around 700^0C the sample was annealed and Au-Si droplets were formed inside the SiO_2

windows (Fig. 2.5e). This is because the mixing of Au with Si reduces the melting temperature of the alloy (~363˚C) as compared to the alloy constituents. The mixed gas of B_2H_6 and Si_2H_6 was then supplied in the chamber with a controlled flow rate. The gas was absorbed by the Au-Si liquid alloy droplet and became supersaturated and Si atoms precipitate out of the supersaturated liquid-alloy droplet at the liquid-alloy/solid-Si interface, and thus p-Si micro needle with desired doping were grown by VLS method (Fig .2.5f).

2.3.2 Results

p-Si microneedles of different sizes at different doping levels were grown. Fig .2.6 shows a typical (7x6) array of p-type Si microneedles of 48 µm long with a diameter of 2 µm grown by in-situ doping VLS mechanism at 690^0C at the growth pressure of 5×10^{-3} Pa using the ratio of B_2H_6 to Si_2H_6 of 6882 ppm (parts-per-million) for 90 min.

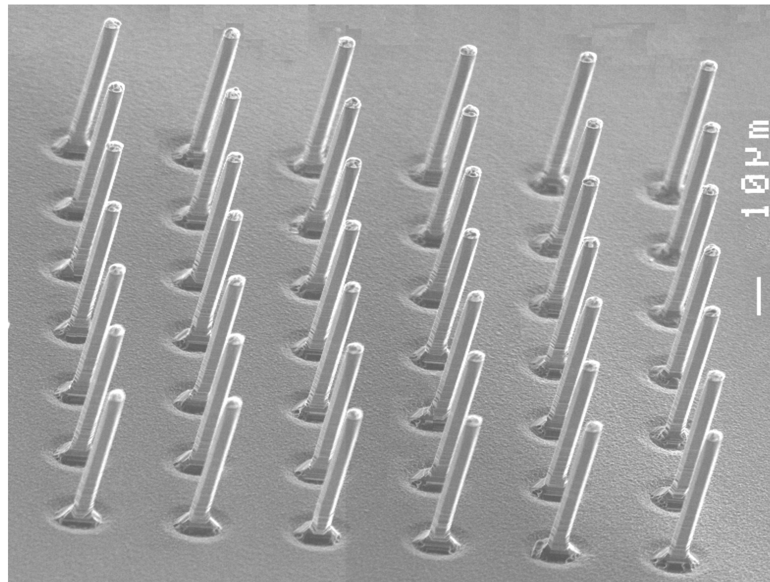

Figure 2.6: SEM image of a typical (7x6) array of p-Si microneedle array grown by *in situ* doped VLS at 690^0C at the growth pressure of 5×10^{-3} Pa using the ratio of B_2H_6 to Si_2H_6 of 6882 ppm for 90 min. [13].

Diameter and length of the microneedles were measured for various sets of experiments (table 2.1). The Current-voltage (I-V) characteristic of boron doped p-Si microneedles were also measured by using one contact with tungsten (W) microneedle at the tip of the p-Si microneedle and the other contact was at the base of the microneedle. For the appropriate placing of the W-needle at the p-Si needle a micromanipulator system was used.

Table 2.1: Experimental data of microneedle growth

B_2H_6 Flow rate (sccm)	SiO_2 Flow rate (sccm)	Temp (C)	Pressure (pa)	Time (min)	Au Dot Diameter (µm)	Needle Length (µm)	Needle Diameter (µm)
0.12	1.7	690^{0}C	5×10^{-3}	90	4	34.81	1.65
					6	36.04	2.47
					8	33.72	2.93
					10	32.77	3.37
0.39	1.7	690^{0}C	5×10^{-3}	90	4	47.74	1.95
					6	47.73	2.56
					8	47.41	3.14
					10	46.37	3.46
0.7	1.7	690^{0}C	5×10^{-3}	90	4	50.20	1.94
					6	50.48	2.49
					8	50.12	3.01
					10	47.80	3.49
1.17	1.7	690^{0}C	5×10^{-3}	90	4	52.31	2.00
					6	53.08	2.62
					8	53.86	3.13
					10	54.24	3.58
1.57	1.7	690^{0}C	5×10^{-3}	90	4	40.41	1.84
					6	38.89	2.35
					8	39.40	2.78
					10	38.57	3.30

CHAPTER 3

Growth Rate Analysis

Chapter 3

Growth Rate Analysis

3.1 Introduction

At first Wagner and Ellis proposed the model of VLS growth in the 1960s [7]. The fundamental part of the model is that the impurity forms a liquid alloy with low melting point. The gas phase molecules preferably condense on the liquid alloy. Microneedle growth occurs because of the precipitation of the growing material from the impurity. In the case of Si needle growth from Au particles the Au-Si forms a eutectic alloy with a melting temperature of 363^0C compared to the individual melting temperatures of Au and Si is 1063^0C and 1412^0C respectively. However the model was for intrinsic type Si microneedle and later it was observed by the researchers that the other factors specially impurity affects the growth rate a lot.

The growth of microneedles by VLS mechanism depends on various factors. Generally the growth rate of microneedles depends on the size of the droplet, the gas flow rate, temperature and pressure and the characteristic of the doping species in case of *in situ* doped VLS etc [14]-[17]. However in this research work only the effect of boron doping level and the droplet size on the growth rate is considered individually while considering the other factors constant.

3.2 Effect of Boron Doping on microneedle growth rate

Intrinsic silicon micro needle can be doped by conventional diffusion process at 1100^0C after VLS growth but *in-situ* doping VLS system can grow doped Si microneedles at lower temperature at around 700^0C. Experimental data shows that the incorporation of doping into VLS system changes the properties of the micro needle compared to the intrinsic one. The modeling of the growth rate of boron doped silicon microneedle grown at low temperature by vapour-liquid-solid (VLS) mechanism is reported here. The mathematical model of the growth rate of silicon micro needle proposed in this work is supported by the experimental values and a complete theoretical analysis is also included.

3.2.1 Experimental Findings

From the Experimental data (Table 3.1) it was found that the growth rate of p-Si microneedle increases with the doping level (B_2H_6 flow rate) for a fixed Au dot size. But this increment in the growth rate gradually slows down and after certain level of doping the growth rate starts to decrease (Figure 3.1)

Table 3.1: Growth rate variation of P-Si microneedle from experimental data with various doping level of P-Si microneedle at a temperature of 700^0C and at the growth pressure of 5×10^{-3} Pa.

B2H6 Flow rate (sccm)	Growth rate(nm/min)
0.12	556
0.7	576
1.2	562
1.57	542

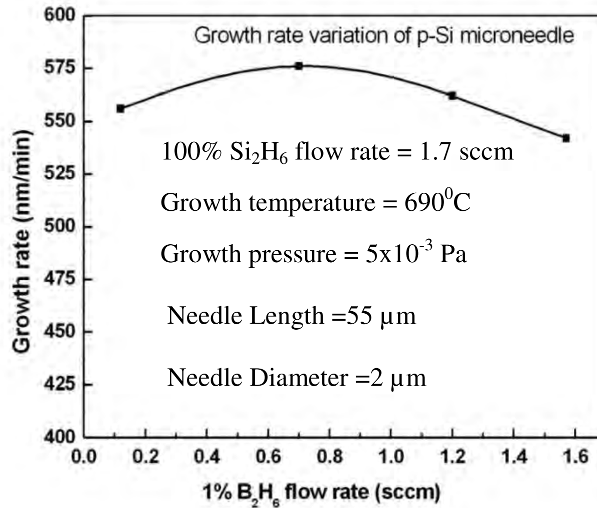

Figure 3.1 : Growth rate variation with doping level of P-Si microneedle grown by VLS at temperature around 700^0C.

3.2.2 Theoretical Analysis

Since the growth rate at first increases then slows down and at last starts to decrease with the increasing B_2H_6 flow rate, it is predicted that there are two effects working behind this nature simultaneously. One effect increases the growth rate and the other one decreases the growth rate. The combination of these two first enhance the growth as the first one dominates and ultimately the growth rate start to decreases as the second cause overpower the first one. From detail study and analysis the following two causes are found which work simultaneously (Fig 3.2) and responsible for the nonlinear growth of the microneedles:

- Sticking property of Boron.
- Loss of Au during VLS growth.

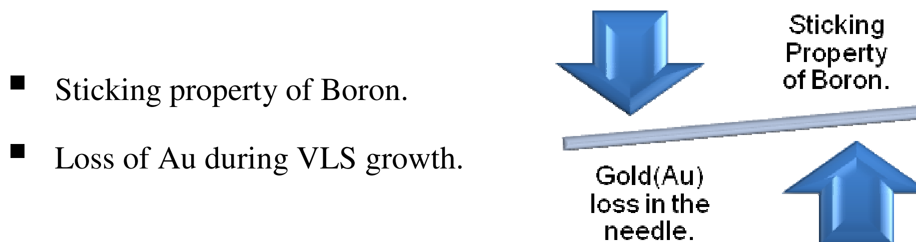

Figure 3.2 : Two effects of boron doping on the growth rate of boron doped Si microneedle.

3.2.2.1 Sticking Property of Boron

The boron has a sticking property as boron is an acceptor atom with three valence band electrons and hence to form covalent bond with Si or other atoms, the lack of one electron make the potential for bond formation much stronger. It is reported that due to this sticking property the growth rate increases linearly with boron doping in Si thin-film by chemical vapor deposition (CVD) method [23]. Although the VLS mechanism is fundamentally different than CVD method, the sticking effect must also be present in boron incorporated VLS system and would be responsible for the growth rate increment of silicon microneedle by VLS method. Therefore boron mixed Au-Si alloy adsorbs more Si_2H_6 and hence enhance the growth rate. However the growth rate is not linear in VLS method as like that in CVD method because of the second effect which is responsible for the decreasing growth rate.

3.2.2.2 Loss of Au during VLS growth.

The second effect is the loss of Au during VLS growth. Ling Pan et al [14] has reported the effect of B_2H_6 on the microstructure of boron doped silicon nanowires (SiNWs) grown by VLS method. It was observed by the group that the structures of undoped or lower B_2H_6 doped SiNWs were different than that of higher B_2H_6 doped SiNWs as in Fig.3.3 (a). In case of higher doping level the nanowire surface roughness was higher, the wires were found to be much shorter than expected and there were lack of Au tips at the ends. That is, the addition of B_2H_6 was responsible for the continuous loss of Au along the growing SiNWs. It is predicted that the loss of Au occurs through the solid defects caused due to the boron doping. The loss of Au was confirmed by observing high-resolution TEM image as shown in Fig. 3.3, where the black dots are gold which is lost during the VLS growth and in the un-doped part of the needle the dots aren’t present.

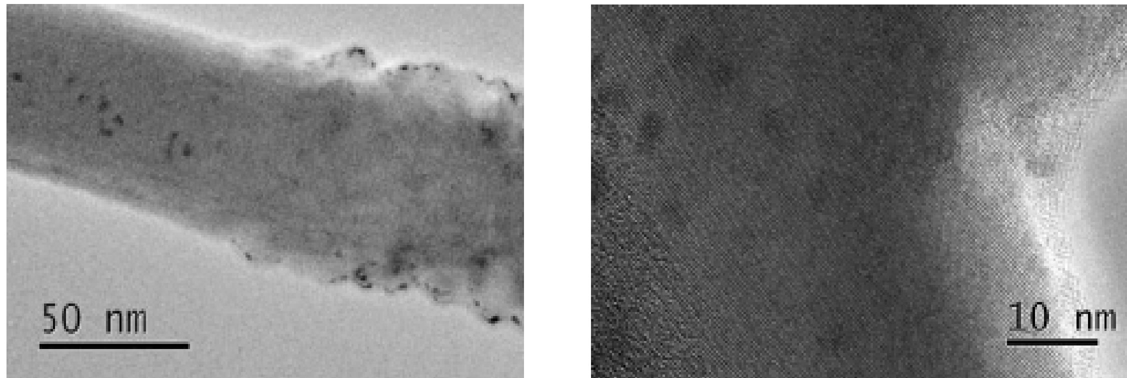

Figure 3.3 : (a) Bright-field TEM images of the undoped-doped transition area of the same nanowire. (b) High-resolution image of the transition area of the nanowire where the darker contrast areas are the Au rich reason. [14]

So it is obvious that at higher B_2H_6 partial pressure i.e. at higher doping level, structural defects in the microneedle increases which is ultimately responsible for the loss of Au within the microneedle during the growth process. However, with the loss of Au in the needle the size of the Au-Si alloy droplet at the top of the needle decreases. As the Au-Si alloy droplet shrinks, the vapour-liquid interface area also decreases which causes less adsorption of Si_2H_6. Thus the growth rate is decreased with the increase of boron doping level.

3.2.3 Mathematical Modelling

For the appropriate mathematical modeling of the growth rate, the aforementioned two effects must be considered simultaneously. Now the first effect of boron doping was linear enhancement in the growth rate [23]. So if we consider only the first effect, the growth rate *(y)* can be expressed as a function of doping level*(x)* with the following equation.

$$y = a + bx$$

Where, a = growth rate without doping

b = adsorption enhancement coefficient for boron doping

Now the second effect, which is present simultaneously with the previous one and responsible for decreasing growth rate, is supposed to be nonlinear. This is because the first effect was linear and hence the second effect has to be nonlinear to make the combined effect nonlinear which was found from the experimental data. As boron doping reduces the size and thus the surface area of the Au-Si droplet, assuming the second order dependency, the growth rate can be related to the doping level by the following equation, considering the second effect only.

$$y = a - cx^2$$

Where, a = growth rate without doping

c = loss coefficient of Au in silicon for boron doping

Now considering these two effects of boron doping a general mathematical model can be established as below.

$$y = a + bx - cx^2 \qquad 3.1$$

Where, a = growth rate without doping

b = adsorption enhancement coefficient for boron doping

c = loss coefficient of Au in silicon for boron doping

These coefficients will be different in different experimental setup but once all the settings such as temperature, pressure etc are settled the coefficients will be constant for the setup. The coefficients can be found for an experimental setup by experimentally collecting one set data first and then by curve fitting for the second order polynomial. Thus measuring the coefficients once, the model proposed in this work will be helpful to predict the growth rate or length of the boron doped silicon microneedle for various doping level. The experimental settings for this model were as below.

Growth temperature = 690^0 C.

Growth Pressure = 5×10^{-3} Pa

100% Si_2H_6 flow rate = 1.7sccm.

The value of the coefficients was found as given below

a = 548.75 unit; b = 69.94 unit; c = 47.65 unit

Fig .3.4 shows the growth rate variation with doping from the model and experimental values and table.3.2 shows the data.

Table 3.2: Growth rate variation of P-Si microneedle from experimental data and from the model.

B2H6 Flow rate (sccm)	Growth rate(nm/min) Experimental Data	Growth rate(nm/min) Data from Model
0.12	556	556
0.7	576	576.016
1.2	562	561.931
1.57	542	542

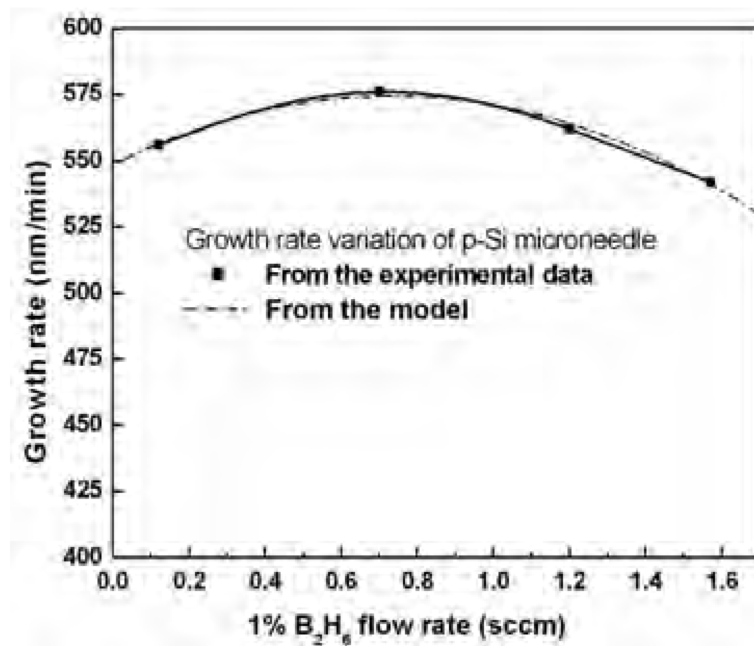

Figure 3.4: Growth rate variation of p-Si microneedle as a function of doping, grown by VLS at a temperature of 690^0C and at the growth pressure of 5×10^{-3} Pa.

3.3 Effect of droplet size on microneedle growth rate

The diameter of the microneedle is directly related to the size of the droplet and it is clear that larger droplet will result micrneedle with larger diameter. Now the thickness i.e. the diameter of the microneedle affects the growth rate of the microneedle. Givargizov [24] divided the growth process into three main steps. In the first step, Si precursor molecules are cracked at the surface of the catalyst droplet and Si is incorporated into the droplet. This is the incorporation step, and the rate [atoms/s] by which it proceeds is called the incorporation rate. After the incorporation of Si, Si diffuses through the droplet surface towards the needle droplet interface. This is the diffusion step. In the last step of the process, Si crystallizes at the liquid-solid interface and forms the Si wire. This is the crystallization step; proceeding at a rate [atoms/s] called the crystallization rate. Givargizov neglected the diffusion step, arguing that diffusion through a microscopic droplet is simply too fast to seriously affect the growth velocity and ultimately chose crystallization step as the rate determining step. According to his observation he reported that comparatively thicker needles grow faster than the thinner needles which were supported by Gibbs-Thomson effect. However, if the material transport, diffusion of growth material on the substrate and the needle surface is taken into account, then the result would be different [25]. In this work the experimental findings of diameter dependency on growth rate is analyzed in the following sections of this chapter.

3.3.1 Experimental Findings

Experimental data of the growth-rate of microneedles, having various diameters, was observed carefully (Table 3.3).The diameter of the microneedle grown by VLS mechanism increases with the liquid catalyst droplets size which is controlled by Au dot. For a fixed boron doping level it was observed that the growth rate of the microneedles changes with the needle diameter and in most of the cases the growth rate of microneedles decreases with the microneedle diameter. The plot of growth rate vs. Au dot size for a different set of doping level is shown in Fig 3.5.

Table 3.3: Growth rate for different Au dot size.

B_2H_6 Flow rate 0.12 (sccm)		B_2H_6 Flow rate 0.39 (sccm)		B_2H_6 Flow rate 0.7 (sccm)		B_2H_6 Flow rate 1.17 (sccm)		B_2H_6 Flow rate 1.57 (sccm)	
Au Dot Diameter (µm)	Growth Rate (µm/min)	Au Dot Diameter (µm)	Growth Rate (µm/min)	Au Dot Diameter (µm)	Growth Rate (µm/min)	Au Dot Diameter (µm)	Growth Rate (µm/min)	Au Dot Diameter (µm)	Growth Rate (µm/min)
4	0.39	4	0.53	4	0.56	4	0.58	4	0.45
6	0.4	6	0.53	6	0.56	6	0.59	6	0.43
8	0.37	8	0.527	8	0.56	8	0.6	8	0.44
10	0.36	10	0.515	10	0.53	10	0.6	10	0.43

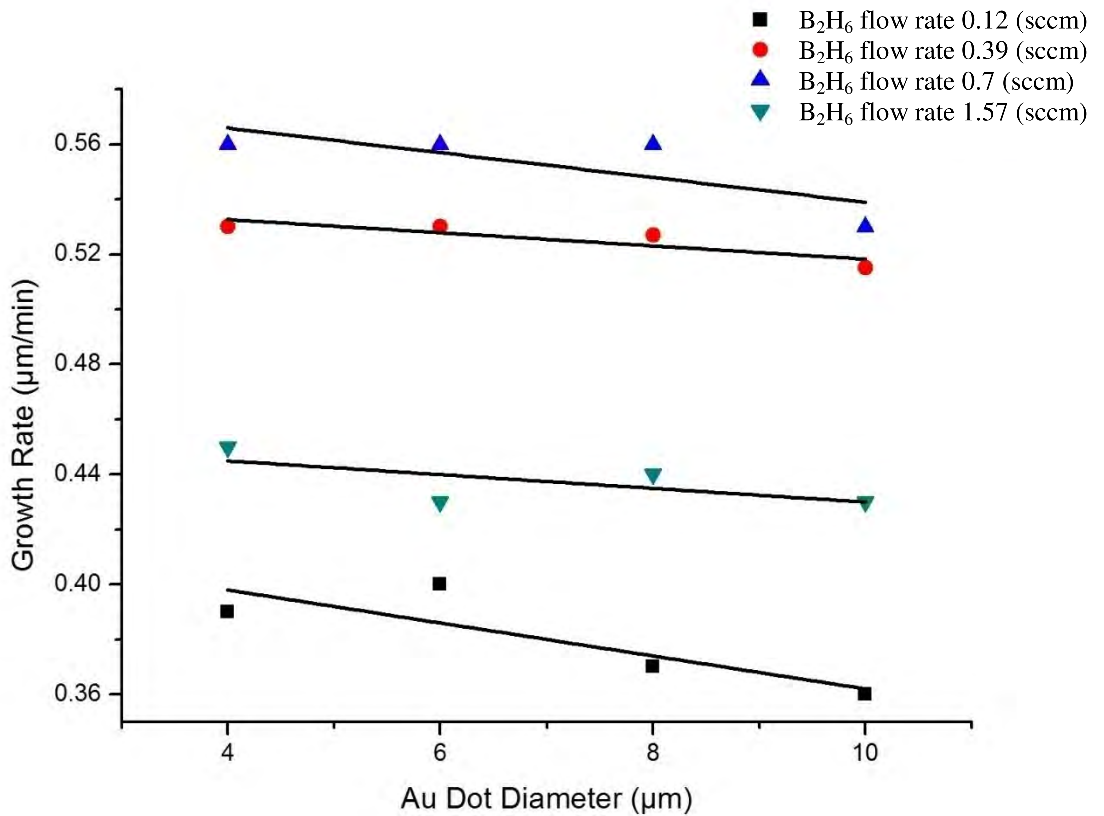

Figure 3.5 : Growth rate (µm/min) Vs Au dot size (µm) for various B_2H_6 Flow rate.

3.3.2.1 Fundamentals of Crystal Growth

The crystal growth process can be divided into four individual steps;

- Adsorption
- Diffusion
- Incorporation
- Desorption

Once adsorbed the adsorbent have the opportunity to diffuse on the surface and reach a preferable position to incorporate. If incorporation isn’t possible within a certain time they get desorbed. The steps are discussed in the following section

- **Adsorption**

The first step of crystal growth is adsorption. The adsorbent material is often introduced as vapor or as a beam. The amount of material that will stick to the surface depends on the property of the adsorbent and the surface. In VLS mechanism the liquid droplet works like a trap and hence the adsorbent prefers to stick to the droplet and hence the growth rate is enhanced. The curvature of the droplet plays an important role on the adsorption knows as Gibbs-Thomson effect which is discussed later.

- **Diffusion**

After adsorption the adsorbent is called monomer or adatom and it can diffuse on the surface for a suitable position to incorporate. The diffusion process is totally random. Diffusion plays an important role in the VLS growth of microneedle. The adatom can diffuse on the substrate surface for a certain amount of time and then either desorption or incorporation can take place.

- **Desorption**

A diffusing monomer always has a probability to get evaporated i.e. desorbed from the surface. The rate of desorption depends on the temperature, pressure,

the surface structure and the monomer characteristics. The desorption rate affects the growth rate in VLS growth method.

- **Incorporation**

The most important part of crystal growth. Diffusion helps the monomers to find a suitable place to make a bond and thus to incorporate to the lattice. The monomer lowers its energy by making bond to the lattice.

3.3.2.2 Gibbs-Thomson Effect

The Gibbs-Thomson effect can be most easily understood by considering a small spherical droplet or particle. The chemical potential μ is the energetic price per atom one has to pay for adding another atom of the same species to the system. For small systems having high surface-to-volume ratios, the influence of the surface on the thermodynamics cannot be neglected. It is evident that increasing the number of atoms (*N)* must necessarily be accompanied by an increase of the surface area and that one has to pay the energetic price for that surface increase as well. When a liquid surface has a curvature the equilibrium vapor pressure increases due to the Gibbs-Thomson effect. The curvature affects the amount of adsorbent which is taken by the droplet. The equation expressing the effect is as follows:

$$\Delta\mu_d = \Delta\mu_\infty - \frac{4\alpha v}{d} \qquad 3.2$$

Where, $\Delta\mu_d$ is the gain of chemical potential.

$\Delta\mu_\infty$ is the gain of chemical potential for a flat surface.

α is vapor-liquid interface energy

υ is the volume of adsorbent atom.

d is the diameter of the droplet.

Here, the driving force for the crystal growth is $\Delta\mu_d$, which is called supersaturation and defined as the difference in chemical potential between vapor phase and the solid(liquid). The larger the difference in chemical potential ($\Delta\mu_d$), the greater is the tendency of phase change from vapor to liquid. Now from the equation it can be said that small diameter decreases the driving forces ($\Delta\mu_d$) and hence the microneedle growth rate is lower. Similarly for larger diameter $\Delta\mu_d$ is larger and hence growth rate is higher. Givargizov also reported such kind of growth characteristics [24]. However, this explanation isn't appropriate in all cases as it deals with only pure intrinsic microneedles and if other impurity is introduced i.e. group III/V materials the different behavior might be obtained.[25]. The following section will reveal the fact.

3.3.2.3 Diffusion Effect

J. Johansson et al [25] presented a mass transport model based on surface diffusion for nanowire growth and observed that for group III/V materials thinner nanowires are longer than thicker ones (Figure. 3.6).

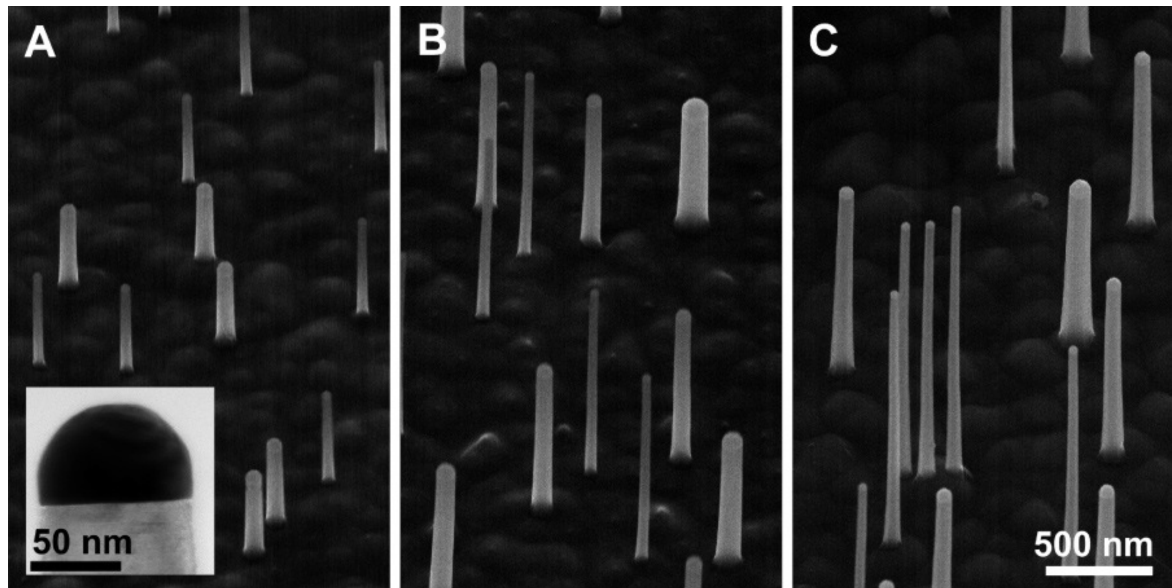

Figure 3.6 : Scanning electron micrographs of GaP nanowires grown with MOVPE at different temperatures: (A) 440 °C, (B) 470 °C, and (C) 500°C [25].

They also demonstrated that Gibbs-Thomson effect can be neglected in such case. According to the model there is steady-state adatom diffusion on the substrate and nanowire side towards the metal and the growth rate depends on the following three factors:

1. The diffusion of material directly deposited on the nanowire side.
2. The adatom diffusion from the substrate surface up along the nanowire.
3. The material directly deposited on the droplet.

The growth rate equation of the mass transport model is as bellows

$$\frac{dL}{dt} = 2R(1 + \frac{\lambda_w}{r_w}) \qquad 3.3$$

Where, L is the length of the nanowire.

R is the deposition rate on the nanowire side and on the droplet.

λ_w represents the diffusion length along the side of the nanowire.

r_w represents the radius of the nanowire.

The equation is valid for L >> λ_w. From the above equation it is clear that the growth rate for needles with larger diameter are lower than the needles with smaller diameters.

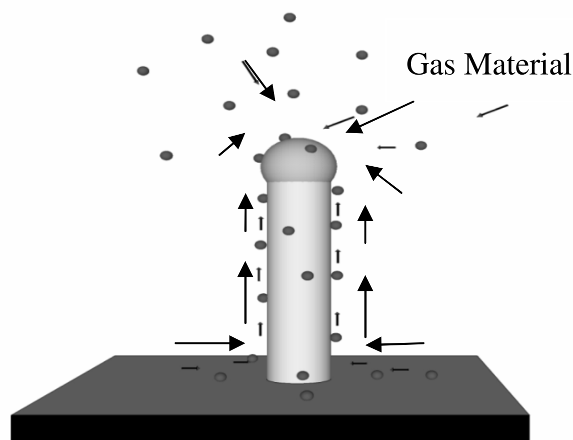

Figure 3.7: Contribution of diffusion in needle growth

3.3.3 Combining the Gibbs-Thomson effect and Diffusion effect

The observation of the experimental microneedles grown by *in situ* doped VLS method shows that in most of the cases the growth rate of thicker microneedles is lower (Figure.3.5). The phenomenon is explained in this section using both the Gibbs-Thomson effect and Diffusion effect. To incorporate Gibbs Thomson effect the shape of the droplet i.e. the diameter and the contact angle need to be examined first. Fig.3.7 shows a close view of a experimentally grown boron doped Si microneedle. It is evident

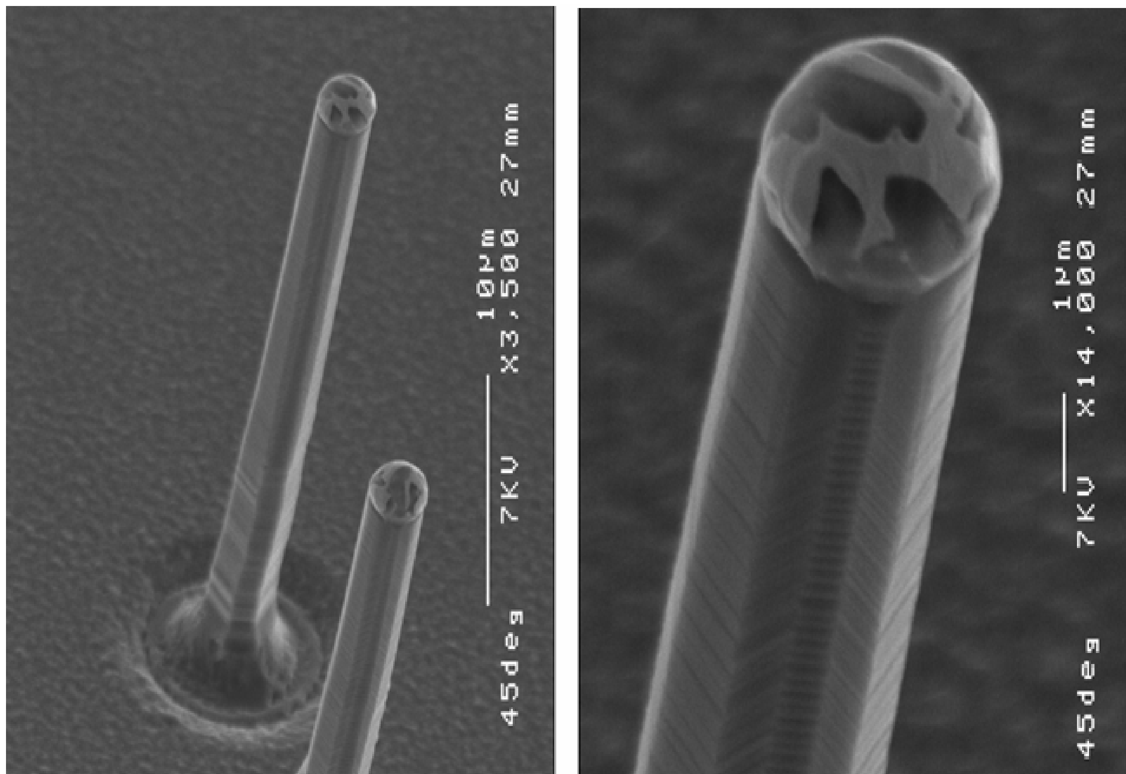

Figure 3.8: experimentally grown boron doped Si microneedle

that there is a diameter expansion at the base where it is attached to the substrate. Givargizov concluded that the "conical expansion at the whisker root is evidently related to a change of the contact angle configuration" [24]. Now it is obvious that the droplet has to undergo some sort of transition in the initial phase of growth, and it is the change of the droplet shape. The Figure3.9 shows the phenomenon.

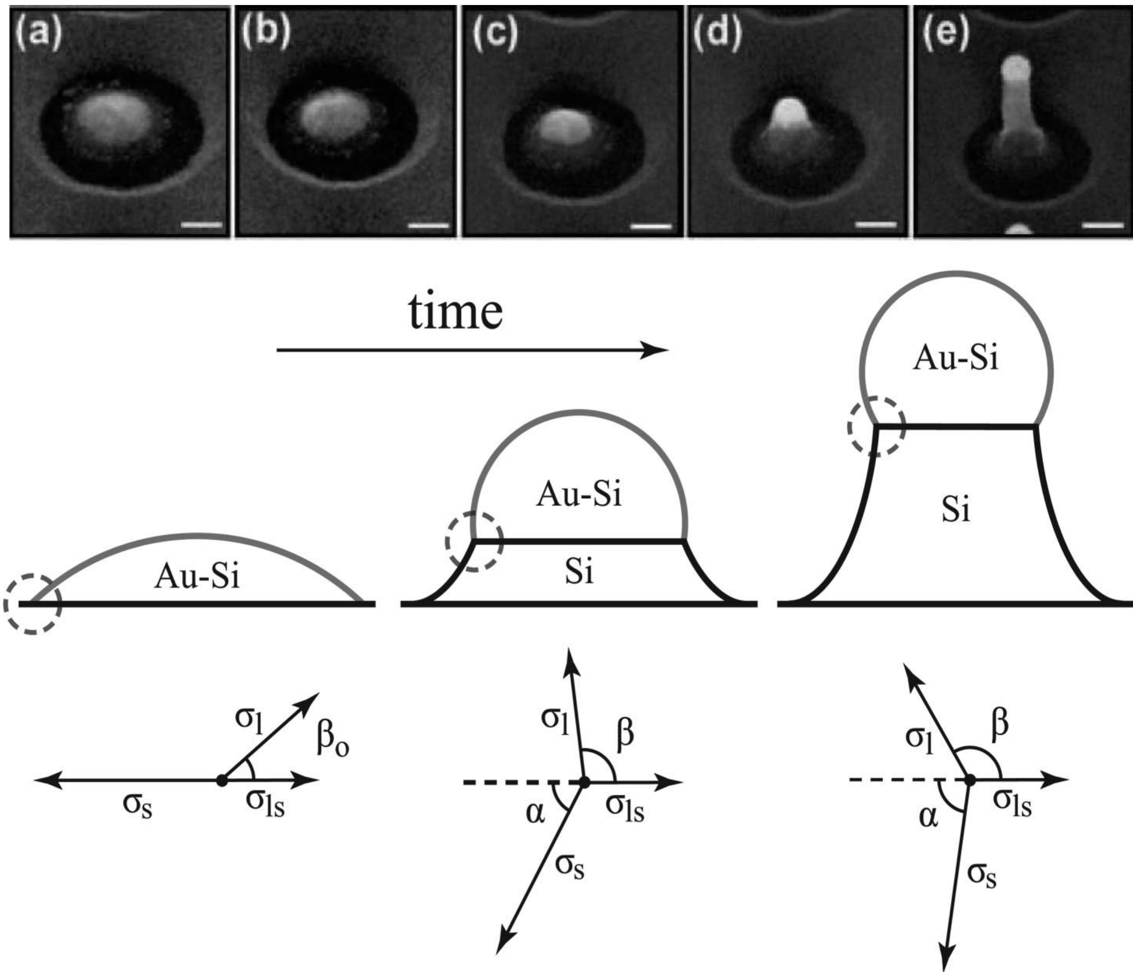

Figure 3.9 : Top: Scanning electron micrographs indicating the development of the droplet shape in the initial phase of growth [26]. Center: Schematic development of droplet and wire shape in the initial phase of growth.. Bottom: the corresponding equilibrium balance of surface forces at the left edge of the droplet (dashed circles).

Now, the amount of silicon which is taken by the droplet is proportional to the vapor-droplet interface area and hence the vapor liquid interface area is needed to be derived as a function of contact angle to find out the growth rate. The Au-Si droplets on top of needles are much more spherical, typically exhibiting contact angle of 90-120° [27]. Figure 3.10 shows such spherical droplet with a contact angle $\beta>90^0$ and radius "r" on a needle with radius "r_0", which will be used for the derivation.

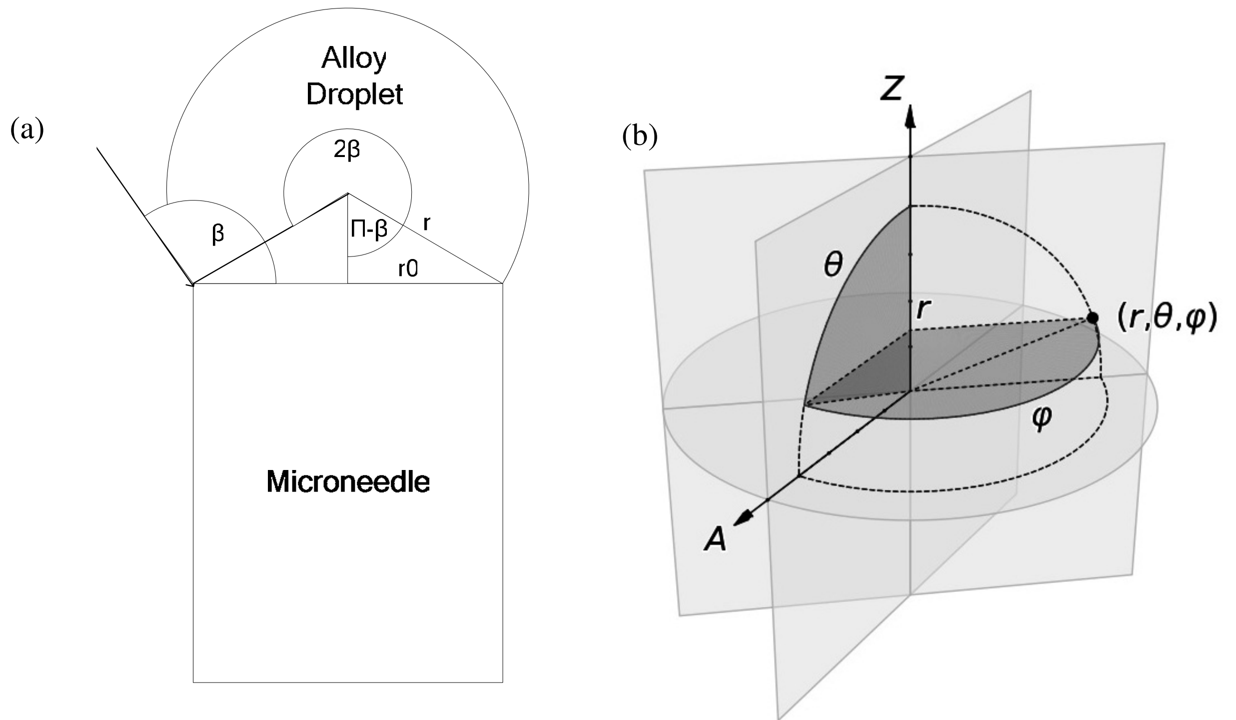

Figure 3.10: (a) Au-si alloy droplet on Si microneedle (β>90^0) (b) spherical coordinate system.

The total area of a sphere from spherical coordinate system by integration is as follows:

$$A=\int_0^{2\pi}\int_0^{\pi} r^2\sin\theta d\theta d\varphi = 4\pi r^2 \qquad 3.4$$

The derivation below is done in case of contact angle β>90^0 by spherical coordinate system. Area of the Alloy droplet (Vapor Liquid interface area)

$= A_{vl}$

$$=\int_0^{2\pi-(2\pi-2\beta)}\int_0^{\pi} r^2\sin\theta d\theta d\varphi$$

$$=r^2\int_0^{2\beta}[-\cos\theta]d\varphi$$

$$=2r^2\int_0^{2\beta}d\varphi$$

$$=4\beta r^2$$

$$=\frac{4\beta r_0^2}{\sin^2\beta} \qquad \because r_0 = r\sin\beta \qquad 3.5$$

Again, the amount of Si which is deposited on the liquid solid interface is proportional to that area, which is,

$$A_{ls} = \pi r_0^2$$

Now if we neglect the contribution of the diffusion effect on the growth rate, the growth rate is proportional to the supersaturation $\Delta\mu_d$, vapor liquid interface area A_{vl} and inversely proportional to the liquid solid interface area A_{ls}.

$$\text{So the growth rate } \propto \frac{\Delta\mu_d \left(\frac{4\beta r_0^2}{\sin^2\beta}\right)}{\pi r_0^2} \qquad 3.6$$

$$\text{Or, growth rate } \propto \left(\Delta\mu_\infty - \frac{4\alpha v}{d}\right)\left(\frac{\beta}{\sin^2\beta}\right) \quad \text{, where } \Delta\mu_d = \Delta\mu_\alpha - \frac{4\alpha v}{d}$$

Since for the range of the variation of droplet volume in our investigation is very small, so the change of β with volume may be considered as constant. Then from the above expression it can be said that growth rate will increase if the needle diameter increases i.e. needles will larger diameter grow faster.

However, if the diffusion of growth material on the needle surface is considered, the result will be different. If the areal density of Si adatoms diffusing toward the catalyst droplet is taken to be constant, then the amount of Si per unit time reaching the droplet is proportional to the circumference of the needle ($2\pi r_0$). Moreover, at a given Si supply rate, the growth rate has to be inversely proportional to the needle cross-sectional area (πr_0^2). Combining both, it becomes immediately clear that the growth rate should be inversely proportional to the needle diameter.

$$\text{Hence, the growth rate considering only diffusion effect } \propto \left(\frac{2\pi r_0}{\pi r_0^2}\right)$$

Or, growth rate $\infty(\frac{1}{r_0})$ 3.7

Now considering the both reason, i.e. the direct adsorption into the droplet and diffusion the VLS growth rate equation becomes as follows:

$$\text{Growth rate } = k_1(\Delta\mu_\infty - \frac{4\alpha v}{d})(\frac{\beta}{\sin^2\beta}) + k_2\frac{2}{d} \qquad Q\ r_0 = \frac{d}{2} \tag{3.8}$$

Where, k_1 and k_2 is constant.

CHAPTER 4

Diameter Analysis

Chapter 4

▪ Diameter Analysis

4.1 Introduction

As explained earlier that the first stage of VLS method is the formation of the droplet which starts the growth process. It is obvious that the diameter of the microneedle depends on the size of the droplet more specifically on the liquid-solid interface area. Hence to analyze the diameter it is important to understand the behavior of the droplet and a theory of liquid droplet on solid surface is discussed in this chapter. Again it was also observed in this work from the experimental data that the doping of boron makes the diameter unstable which is also analyzed later.

4.2 Effect of Au dot size on microneedle diameter

In the experiment cylindrical Au dot of certain Au film thickness and different diameters were used to form microneedles having various diameters. It is evident that larger Au dot will form larger droplet and ultimately microneedles with larger diameter.

A theoretical relation between the Au dot size and the microneedle diameter is derived in this work which is compared with the experimental findings.

4.2.1 Experimental Findings

Experimental data shows that if the Au dot diameter is increased keeping the Au film thickness constant, for a fixed doping level the microneedle diameter also increases. The results for different doping level are depicted in Figure 4.1(a) and (b).

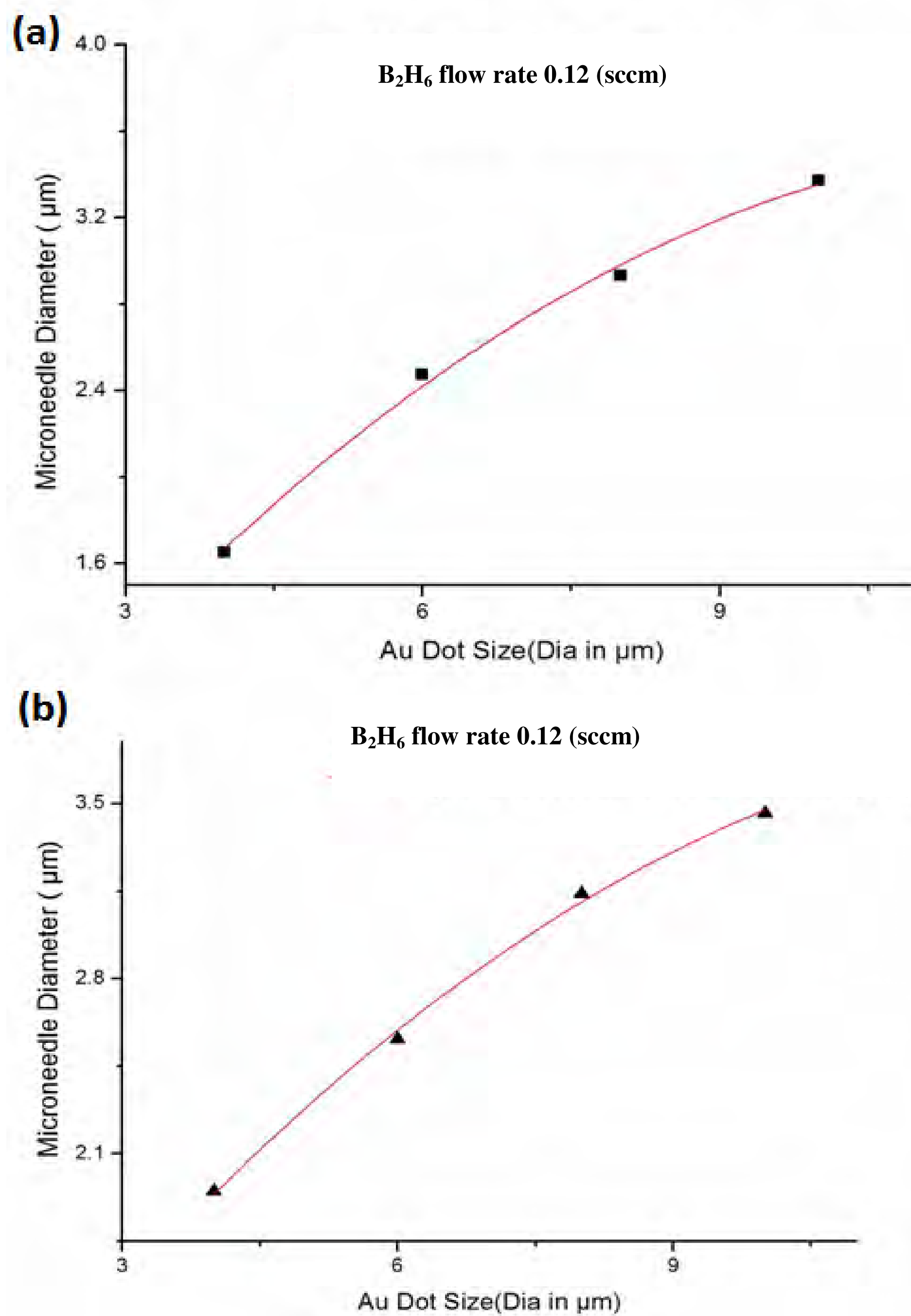

Figure 4.1: Experimental results on Microneedle diameter as a function of Au dot size for B_2H_6 flow rate (a) 0.12 sccm (b) 0.39 sccm .

The graph above shows that the relationship between microneedle diameter and the Au dot diameter is increasing but not liner. The corresponding data is given in table 4.1.

Table 4.1: Microneedle diameter for different Au dot size.

B_2H_6 Flow rate 0.12 (sccm)		B_2H_6 Flow rate 0.39 (sccm)		B_2H_6 Flow rate 0.7 (sccm)		B_2H_6 Flow rate 1.17 (sccm)		B_2H_6 Flow rate 1.57 (sccm)	
Au Dot Diameter (μm)	Needle Diameter (μm)	Au Dot Diameter (μm)	Needle Diameter (μm)	Au Dot Diameter (μm)	Needle Diameter (μm)	Au Dot Diameter (μm)	Needle Diameter (μm)	Au Dot Diameter (μm)	Needle Diameter (μm)
4	1.65	4	1.95	4	1.94	4	2	4	1.84
6	2.47	6	2.56	6	2.49	6	2.62	6	2.35
8	2.93	8	3.14	8	3.01	8	3.13	8	2.78
10	3.37	10	3.46	10	3.49	10	3.58	10	3.3

4.2.2 Theoretical Analysis

The shape of the Au dot is like a cylinder as described in the fabrication process in section 2.3.1. Au-Si alloy forms when the Au dot is heated on the Si surface at temperature higher than the eutectic temperature. The alloying process is explained in detail in section 2.2.3.1. The percent of Silicon mix with the gold depends on the temperature and the percent can be measured from Au-Si binary phase diagram (Fig.2.3). So it can be said that the volume of the Au-Si droplet is proportional to the Au dot volume. From this relation the relation between the Au dot diameter and the microneedle diameter can be found.

4.2.3 Mathematical Relation

To derive the relation the following assumption is considered

- The Au dot is cylindrical in shape.
- Radial transverse growth of microneedle diameter due to Vapor Solid (VS) mechanism is negligible.
- The microneedle diameter is constant during the growth process(Neglecting the effect of Au loss).

The contact angle of the droplet on the top of the microneedle is greater than 90^0 which is shown in the section 3.3.3 and to find out the volume of the droplet we will use the

Figure.3.10 and the equation of the liquid vapor interface area A_{vl} as derived in section 3.3.3 of Chapter 3 of the book. Thus the volume of spherical droplet with a contact angle $\beta>90^0$ and radius "r" on a needle with radius "r_0" can be derived is as bellows:

Volume of the Alloy droplet $V_{Au\text{-}Si}$ =

$$= \int_0^r A(r)dr$$

$$= \int_0^r 4\beta r^2 dr$$

$$= \frac{4}{3}\beta r^3$$

$$= \frac{\frac{4}{3}\beta r_0^3}{\sin^3\beta} \qquad Q\ r_0 = r\sin\beta \qquad 4.1$$

Now, the volume of a with diameter "x" and height h is

$V_{Au}=\pi(x/2)^2h$.

Now, as the volume of the Au-Si droplet is proportional to the Au dot volume

$$\frac{\frac{4}{3}\beta r_0^3}{\sin^3\beta} \infty \pi(\frac{x}{2})^2 h$$

If the contact angle 'β' and Au dot height 'h' is constant, the relation will be

$d_0^3 \infty x^2$ Where, $d_0=2r_0$ is the diameter of the needle.

Or, $d_0 \infty x^{\frac{2}{3}}$

Or, $d_0 = kx^{\frac{2}{3}}$ where, k is a constant. 4.2

Now, if we draw the curve from the above relation for an arbitrary value of k=0.75 the relationship almost matches the experimental findings (Figure.4.1).

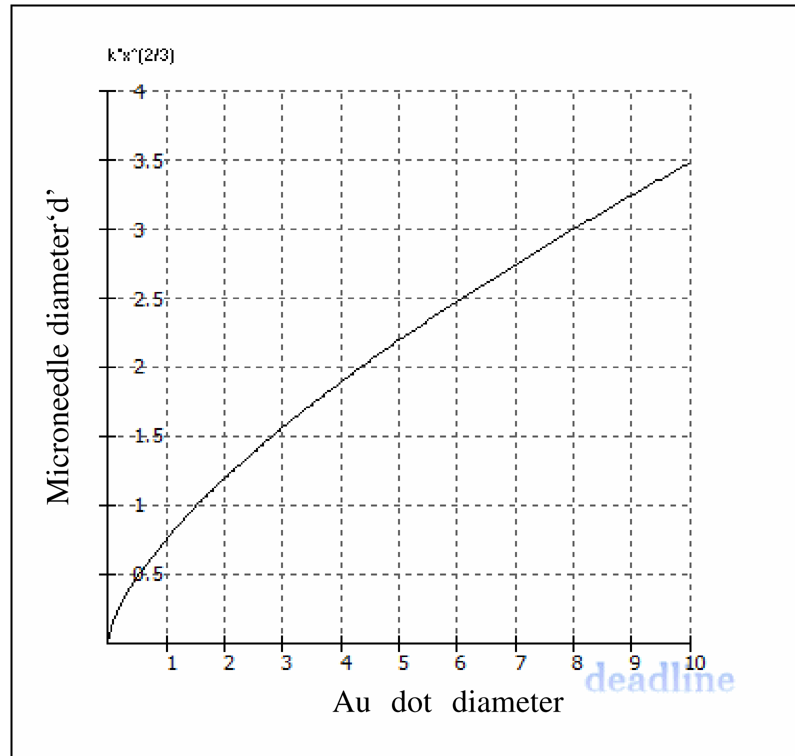

Figure 4.2 : Theoretical relation between Microneedle diameter and Au dot diameter.

4.3 Effect of doping on microneedle diameter

It is already reported that boron doping has a severe affect on the growth rate of the microneedle[12] and here the effect of doping on microneedle diameter will be analyzed based on the experimental findings. The incorporation of Boron must have an effect on the surface roughness and the sticking property of Boron enhances Si adsorption (sec 3.2.2.1). These will ultimately change the property and shape of the Au-Si alloy droplet and thus affect the diameter of the microneedle.

4.3.1 Experimental Findings

Experimental result shows that for a certain Au dot size if the doping level is increased the diameter of the microneedle deviates about 0.2µm-0.3 µm and seems to

have a periodic relation with the doping. The graph and corresponding data table is given below.

Table 4.2: Experimental data for microneedle diameter for different doping level.

Au Dot Diameter (4 µm)		Au Dot Diameter (6 µm)		Au Dot Diameter (8 µm)		Au Dot Diameter (10 µm)	
B_2H_6 Flow rate (sccm)	Needle Diameter (µm)	B_2H_6 Flow rate (sccm)	Needle Diameter (µm)	B_2H_6 Flow rate (sccm)	Needle Diameter (µm)	B_2H_6 Flow rate (sccm)	Needle Diameter (µm)
0.12	1.65	0.12	2.47	0.12	2.93	0.12	3.37
0.39	1.95	0.39	2.56	0.39	3.14	0.39	3.46
0.7	1.94	0.7	2.49	0.7	3.01	0.7	3.49
1.17	2	1.17	2.62	1.17	3.13	1.17	3.58
1.57	1.84	1.57	2.35	1.57	2.78	1.57	3.3

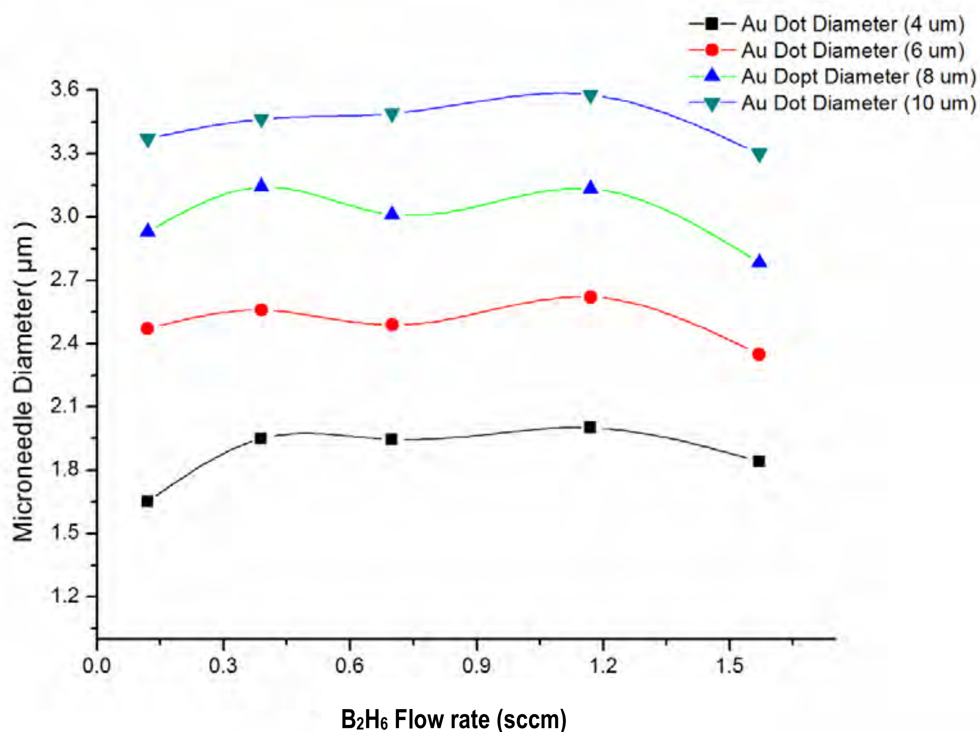

Figure 4.3: Microneedle diameter Vs doping level.

4.3.2 Theoretical Analysis

The diameter of the microneedle is determined by the liquid solid interface area and hence it is important to find out the initial spreading of Au-Si alloy droplet on the substrate. Au-Si alloy droplets on flat Si substrates and at temperatures of 400-650 °C show a contact angle (defined here as the angle within the liquid) of about ≈ 43° [28]. As the experiment in this work was done at 700^0C we can assume the initial contact angle of the alloy (inside) $\beta<90^0$. B. Ressel et al also reported such result of contact angle which is shown in Figure 4.4[18]. This low value of contact angle indicates a strong liquid–solid interaction and means that the liquid droplet tends to spread on the solid substrate.

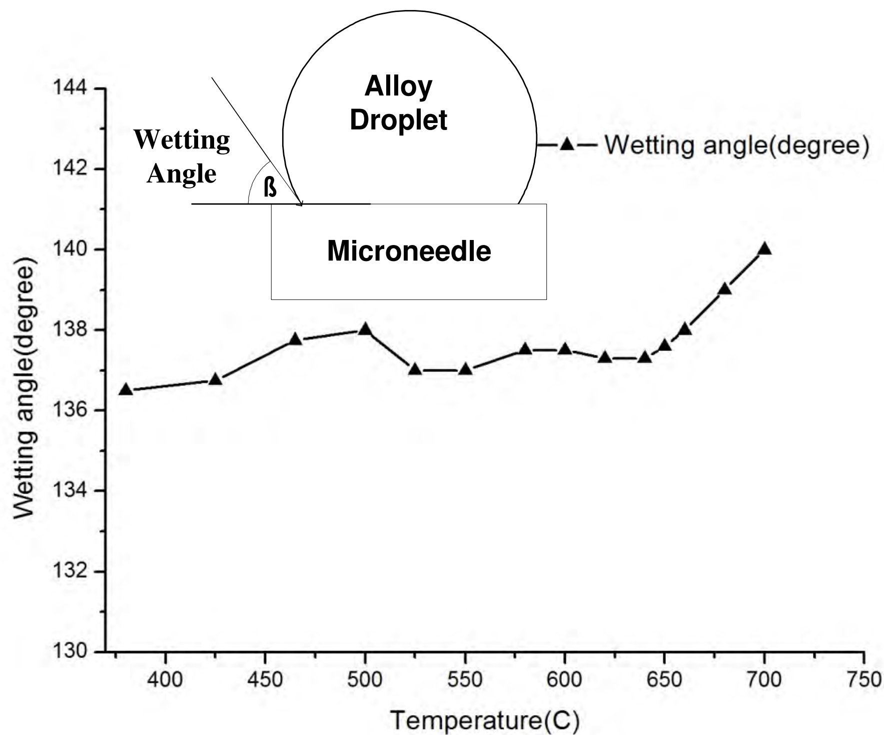

Figure 4.4 : Contact angle (measured in the gas phase) as a function of temperature.[18]

T. Young was the first to describe contact angle equilibrium. The vector summation of forces at the three-phase intersection point gives the Young's equation.

$$\gamma_{SV} = \gamma_{SL} + \gamma_{LV} \cos\beta \qquad 4.3$$

Where, γ is the surface tension (or surface free energy).

γ_{SV} is the interfacial tensions, between solid and vapor.

γ_{SL} is the interfacial tensions, between solid and Liquid.

γ_{LV} is the interfacial tensions, between liquid and vapor.

The figure of a droplet at equilibrium is shown in figure 4.5. Now the surface roughness depends on the mole fraction of Si in the droplet. [18]. If the mole fraction increases the

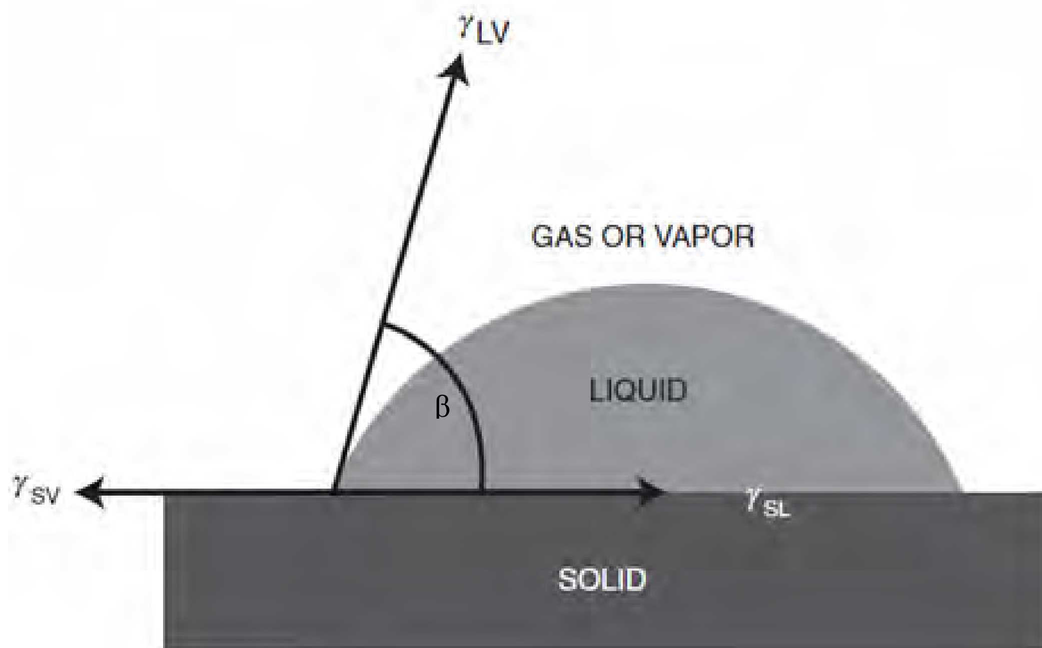

Figure 4.5: Vectorial equilibrium for a droplet of a liquid resting on a solid.

surface roughness also increases. The roughness of the liquid-solid interface affects the interface tension at the liquid-solid interface and the vapor-solid interface. Again if the surface of a substrate is rough, then the actual surface area is greater than the plane(flat) surface area and therefore for a given droplet volume, the total liquid–solid interaction is greater on the rough surface than on a flat surface. If the smooth material gives a contact angle greater than 90°, the presence of surface roughness increases this angle still further, but if β is less than 90°, the increase in surface roughness decreases the angle which is the case of Au-Si droplet. If the surface roughness 'r_w' is combined with Young's equation the expression of contact angle can be written as bellows.[29]

$$\cos\beta' = r_w\left(\frac{\gamma_{SV} - \gamma_{SL}}{\gamma_{LV}}\right) \qquad 4.4$$

The periodic change in the microneedle diameter as a function of doping level now can be explained considering both positive and negative effect.

First, let's consider the positive effect: If the doping level is increased due to the sticking property of Boron (discussed in section 3.2.2.1) mole fraction of Si in the droplet increases, the surface roughness increases, contact angle decreases (Equation 4.4) i.e. the droplet spreads more on the substrate and ultimately the diameter increases.

Now let us look at the negative effect: If the doping level is increased, the gold loss in the substrate increases [14], mole fraction of Si in the droplet decreases, surface roughness decreases, contact angle increases i.e. the droplet spreads less on the substrate and ultimately the diameter decreases. Diameter also decreases if the volume of the droplet decreases due to gold loss.

When the positive effect is superior to the negative one, the droplet will expand. On the other hand if the negative effect dominates the diameter will shrink.

CHAPTER 5

Metal-Semiconductor Junction Theory

Chapter 5

Metal-Semiconductor Junction Theory

5.1 Introduction

Metal-semiconductor contacts have been known to have rectifying properties since 1874. The theory of metal-semiconductor contacts is attributed to Schottky (1938). Today, specially manufactured Schottky diodes are often used in rectification since they have a smaller forward voltage drop than p-n junction rectifiers. The shottky-barrier diode is formed by a metal contact (anode) to a semiconductor (the cathode), instead of the more common junction between p-type and n-type semiconductors. Shottky diodes differ from pn-junction devices in that rectification occurs because of differ in work function between the metal contact and the semiconductor, rather a nonuniform doping profile. Conduction is not controlled by minority carrier recombination in the semiconductor, but by thermionic emission of majority carriers over the barrier created by the unequal work functions. The Schottky diode is, therefore, a majority carrier device whose switching speed is not limited by minority carrier effects. There is also the problem of making metallic contacts to semiconductors, where a rectifying action is not wanted. The Schottky theory also permits the identification of the conditions necessary for the preparation for ohmic (as opposed to rectifying) metal contacts on semiconductors.

5.2 Metal-Semiconductor Junction

When the metal and semiconductor are in equilibrium and are not in contact, the energy levels are constant throughout the materials (Figure.5.1). The Fermi levels are generally unequal, indicating that the electrons in one material (in this case the metal) have less energy, on the average, than these in the semiconductor. Therefore, when the materials are joined, some of the electrons in the semiconductor move spontaneously into the metal and collect on the surface (Figure.5.2). These leave behind ionized donor locations, which are positively charged, and create a negative surface charge where they collect on the surface of the metal. An electric field is set up between these positive charges in n-semiconductor and the electrons in metal. The direction of the field would be form n-semiconductor to metal that eventually inhibit further electron flow into the metal. The positively charged region is called a depletion region, since it is almost completely depleted of mobile electrons. The shape of the energy diagram of the metal-semiconductor junction is governed by the following three rules:

- In equilibrium, the Fermi levels for the semiconductor and metal must be constant throughout the system;
- The electron affinity must be constant;
- The free-space energy level must be continuous.

However, the barrier which is formed in the interface is responsible for controlling the current flow. The band diagram in case of metal and n-type semiconductor before and after contact is shown in the following figures.

Band Diagram (before contact)

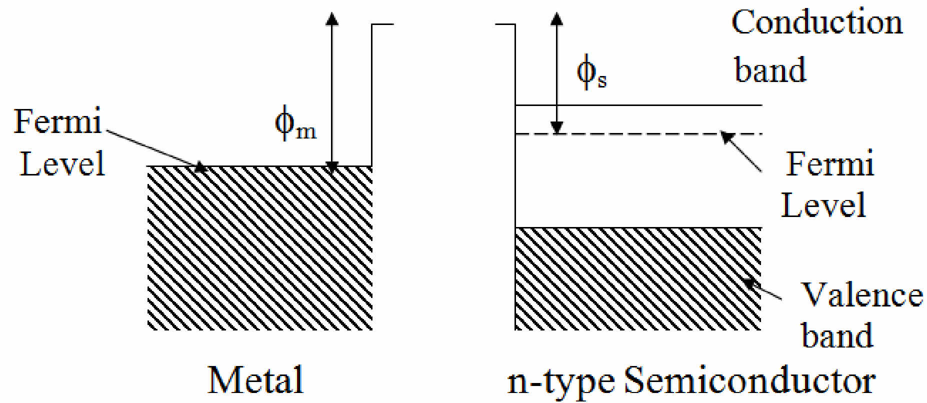

Figure 5.1: Band diagram of metal and n-type semiconductor before contact

Where,

ϕ_m - work function of metal

ϕ_s - work function of semiconductor

If $\phi_m > \phi_s$ (as drawn), electrons flow from semiconductor to metal.

Band diagram (after contact)

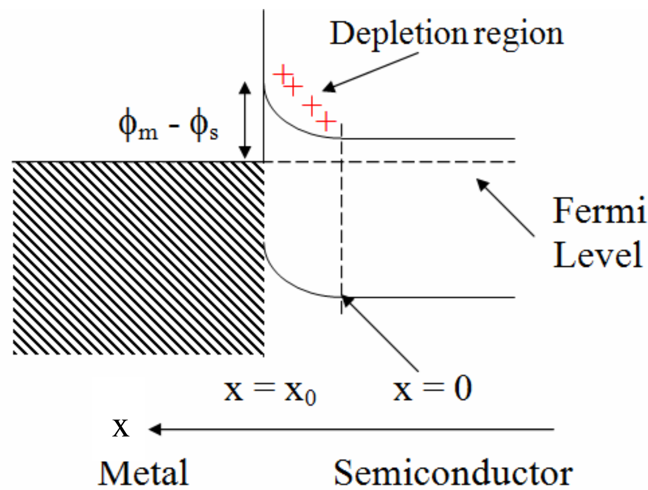

Figure 5.2: Band diagram of metal and n-type semiconductor after contact

5.3 Ideal case of Barrier height

For a metal, the energy required to remove an electron into the "vacuum" is given by the work function ϕ_m and the equivalent measure for the semiconductor is the electron affinity χ_s.

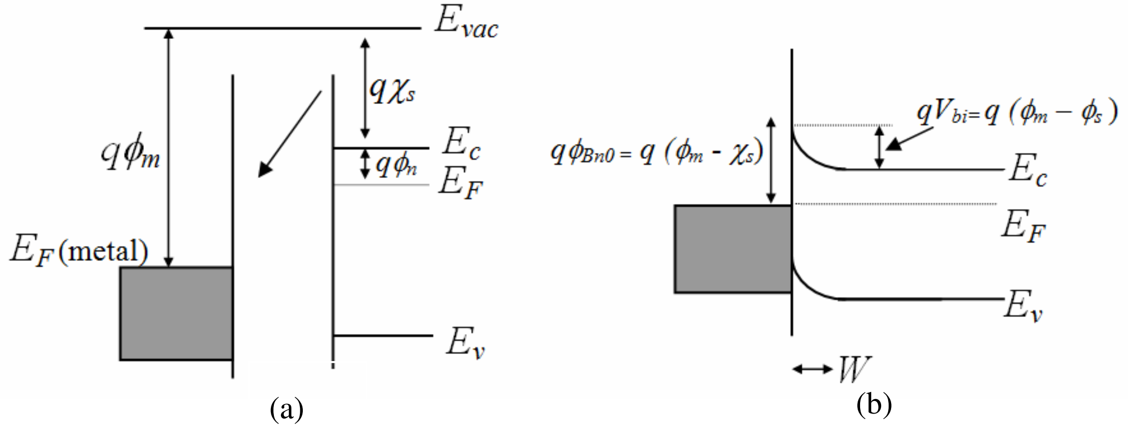

Figure 5.3: Electronic energy relations of a high work-function metal and an n-type semiconductor

Figure 5.3(a) shows the electronic energy relations of a high work-function metal and an n-type semiconductor which are not in contact and are in separate systems. If the two are allowed to contact with each other, charge will flow from the semiconductor to the metal and equilibrium is established as a single system. The Fermi levels on both sides will line up. Relative to the Fermi level in the metal, the Fermi level in the semiconductor is lowered by an amount equal to the difference between the two work functions. As mentioned earlier the work function is denoted by ϕ_m for the metal, and is equal to $q(\chi_s + \phi_n)$ for the semiconductor, where $q\chi_s$ is the electron affinity measured from the bottom of the conduction band Ec, to the vacuum level, and $q\phi_n$ is the energy difference between E_C, and the Fermi level. The potential difference between the two work functions $\phi_m - (\chi_s + \phi_n)$ is called the contact potential. From figure 5.3(b) it is clear that the barrier height is simply the difference between the metal work function and the electron affinity of the semiconductor. For an ideal contact between a metal and a n-type semiconductor, the barrier height $q\phi_{Bno}$ is given by $q\phi_{Bno} = q(\phi_m - \chi_s)$ and for a p-type semiconductor, the barrier height $q\phi_{Bpo}$ is given by $q\phi_{Bpo} = E_g - q(\phi_m - \chi_s)$.

5.4 Junction Under Biasing

Figure 5.4 shows Energy-band diagrams of metal on n-type (left) and on p-type (right) semiconductors under different biasing conditions. In case of a metal-n type semiconductor junction, a forward bias consists of making the metal positive and the semiconductor negative, which lowers the barrier.

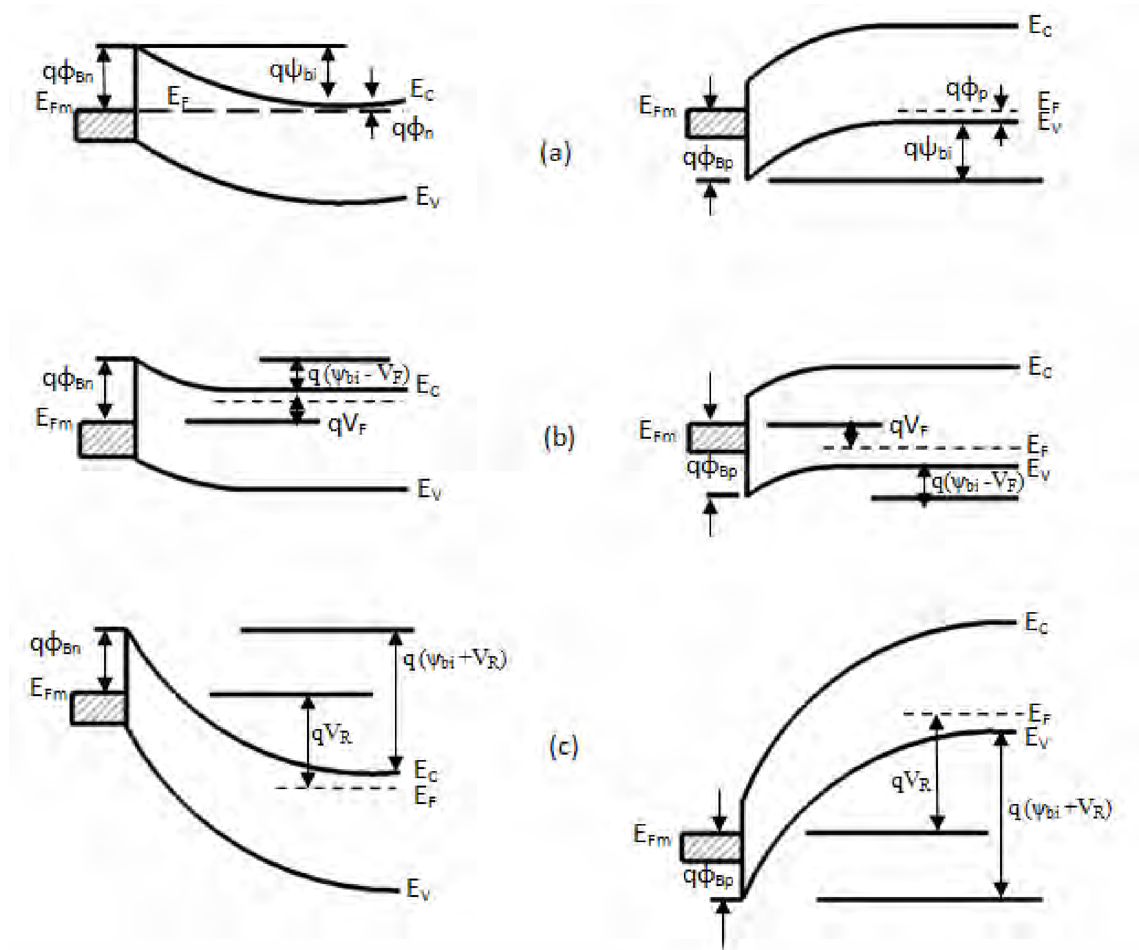

Figure 5.4: Energy-band diagrams of metal on n-type (left) and on p-type (right) semiconductors under different biasing conditions. (a) Thermal equilibrium. (b) Forward bias. (c) Reverse bias.[30]

This increases the electron current injected from the semiconductor into the metal. Reverse bias raises the barrier and decreases the injected electron current. In case of metal-p type semiconductor junction, a forward bias consists of making the metal

negative and the semiconductor positive and in that case holes are attracted to the interface. This results in reduced depletion region and barrier and a large net current. Conversely reverse bias causes increased depletion region and barrier height which results about zero net current.

5.5 Current Transport Method

Discussion of the current through the junction is however very different from the bipolar junction. Figure 5.5 shows five fundamental transport processes under forward bias.

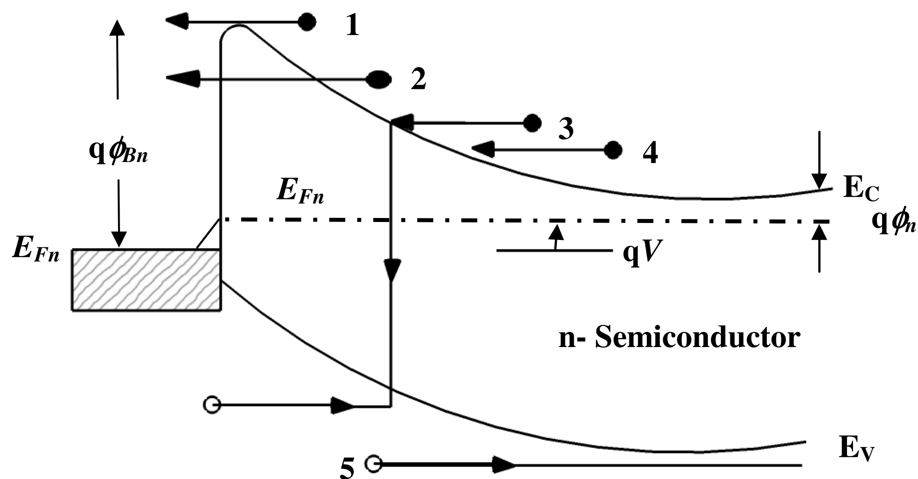

Figure 5.5:Five fundamental transport processes under forward bias. (1) Thermionic emission. (2) Tunneling. (3) Recombination. (4) Diffusion of electrons. (5) Diffusion of holes.[30].

The five basic current transport processes are:

1. Emission of electrons from the semiconductor over the potential barrier into the metal.
2. Quantum mechanical tunneling of electrons through the barrier.
3. Recombination in the space-charge region.
4. Diffusion of electrons in the depletion region.
5. Holes injected from the metal that diffuse into the semiconductor.

The first one is the dominant process for Schottky diodes with moderately doped semiconductors. The second process tunneling is important for heavily doped semiconductors and responsible for most ohmic contacts. In addition, edge leakage current may occur due to a high electric field at the metal-contact periphery or interface current due to traps at the metal-semiconductor interface. The main contribution to the current through the junction is caused by electrons thermally overcoming or tunneling through the barrier. Thermionic emission is the most important contribution to the device current under moderate electric fields and hence the thermionic emission theory will be discussed in detail in the following section of this chapter.

5.6 Thermionic emission theory

Thermionic emission across a metal-semiconductor junction is similar to thermionic emission from a metal into the vacuum, except that the appropriate electron density functions and electric field values are used. The theory was given by Bethe which is derived from the following assumptions:

- The barrier height $q\phi_{Bn}$ is much larger than kT.
- Thermal equilibrium is established at the plane that determines emission, and
- The existence of a net current flow does not affect this equilibrium.

The case for a Schottky junction is considered here. The current density across such a barrier from semiconductor to metal $J_{s\to m}$ is given by the number of electrons with energies sufficient to overcome the barrier.

$$J_{s\rightarrow m} = \int_{E_{Fn}+q\phi_{Bn}}^{\infty} qv_x dn \qquad 5.1$$

Where, v_x is the velocity of the electrons in the direction of the transport, and $E_{Fn} + q\phi_{Bn}$ is the minimum energy for thermionic emission into the metal. Now the electron density is given by

$$dn = N(E)F(E)dE \qquad 5.2$$

Where, *N (E)* being the density of states and *F(E)* the Fermi-Dirac distribution function. Using the usual approximations for *F(E)* and *N(E)*:

$$dn = \frac{4\pi\left(2m^*\right)^{3/2}}{h^3}\left(E - E_C\right)^{1/2} e^{\frac{E-E_C+q\phi_n}{kT}} dE \qquad 5.3$$

Now, if we further assume that all the energy of the conduction-band electrons is kinetic energy, then

$$\begin{aligned} &\left(E - E_C\right) = \tfrac{1}{2} m^* v^2 \\ &dE = m^* v dv \\ &\sqrt{E - E_C} = v\sqrt{\frac{m^*}{2}} \end{aligned} \qquad 5.4$$

Where, v is the total electron velocity ($v^2 = v_x^2 + v_y^2 + v_z^2$)

Substituting Eqs.5.4 into Eq.5.3 gives,

$$dn \approx 2\left(\frac{m^*}{h}\right)^3 e^{-\frac{m^* v^2}{2kT}} e^{-\frac{q\phi_n}{kT}} \left(4\pi v^2\right) dv \qquad 5.5$$

Using the standard transformation $4\pi v^2 dv = dv_x\ dv_y dv_z$, and letting v_{ox} be the velocity corresponding to just overcoming the barrier,

$$J_{s\rightarrow m} = 2q\left(\frac{m^*}{h}\right)^3 e^{-\frac{q\phi_n}{kT}} \int_{v_{ox}}^{\infty} v_x e^{-\frac{m^* v_x^2}{2kT}} dv_x \int_{-\infty}^{\infty} e^{-\frac{m^* v_y^2}{2kT}} dv_y \int_{-\infty}^{\infty} e^{-\frac{m^* v_z^2}{2kT}} dv_z$$

$$= \left(\frac{4\pi\, qm^* k^2}{h^3}\right) T^2\, e^{-\frac{q\phi_n}{kT}} e^{-\frac{m^* v_{ox}^2}{2kT}} \qquad 5.6$$

Now, v_{ox} be the minimum velocity in the x-direction to just overcoming the barrier and is given by,

$$\tfrac{1}{2} m^* v_{ox}{}^2 = q(\psi_{bi} - V) \qquad 5.7$$

Where, ψ_{bi} is the bulk in potential and V is the biasing voltage. Substituting Eq. 5.7 in Eq.5.6 yields

$$J_{s\rightarrow m} = A^* T^2\, e^{-\frac{q\phi_{Bn}}{kT}} e^{\frac{qV}{kT}} \qquad 5.8$$

Here, $A^* = \left(\frac{4\pi\, qm^* k^2}{h^3}\right)$, which is known as Richardson constant for thermionic emission. Now, the total current density is:

$$J = J_{s\rightarrow m} - J_{m\rightarrow s} \qquad 5.9$$

Where, $J_{m\rightarrow s}$ is the reverse current flow that is largely unaffected by the applied potential and hence it must be equal to the current flowing from the semiconductor into the metal when thermal equilibrium prevails at *V=0,* since *it* follows that:

$$J_{m\to s} = J_{s\to m}(V = 0) = J = A^{*}T^{2}\, e^{-\frac{q\phi_{Bn}}{kT}} \qquad 5.10$$

Substituting, the Eq. 5.10 and Eq. 5.8 into Eq. 5.9 the total current density can be found

$$J = A^{*}T^{2}\, e^{-\frac{q\phi_{Bn}}{kT}}\left(e^{\frac{qV}{kT}} - 1\right) \qquad 5.11$$

We therefore have a law similar to that for the p-n junction diode:

$$J = J_{TE}\left(e^{\frac{qV}{kT}} - 1\right) \qquad 5.12$$

Where, $J_{TE} = A^{*}T^{2}\, e^{-\frac{q\phi_{Bn}}{kT}}$

The advantage of Schottky diodes over p-n junction diodes in circuit applications stem from their higher speed (no minority carriers) and lower forward voltage drop (small barrier height). On the other hand they suffer from low reverse breakdown voltages and greater temperature sensitivity of leakage currents.

CHAPTER 6

I-V Characteristic Analysis

Chapter 6

I-V Characteristic Analysis

6.1 Introduction

I-V characteristic of Boron doped p-type Si microneedles, grown by *in situ* doped VLS mechanism was observed. It was found that the incorporation of doping reduces the resistivity of the needles and shows nonlinear I-V characteristic. Mathematical model of the I-V characteristic is proposed in this chapter which is supported by the experimental values and simulation results. This model will be useful while applying needle as a sensor required for certain application.

6.2 Experimental Findings

The Current-voltage (I-V) characteristic of boron doped p-Si microneedle was measured by using one contact with tungsten (W) microneedle at the tip of the p-Si microneedle and the other contact at the base of the microneedle. For the appropriate placing of the W-needle at the p-Si needle a micromanipulator system was used. Fig.6.1 shows a typical J-V characteristic of a microneedle with a length of 38.57 µm and a diameter of 3.30 µm grown by VLS method at of 690^0C and at the growth pressure of 5×10^{-3} Pa for a B_2H_6 flow rate of 1.57 sccm and SiO_2 flow rate of 1.7 sccm. The table 6.1 shows the experimental data.

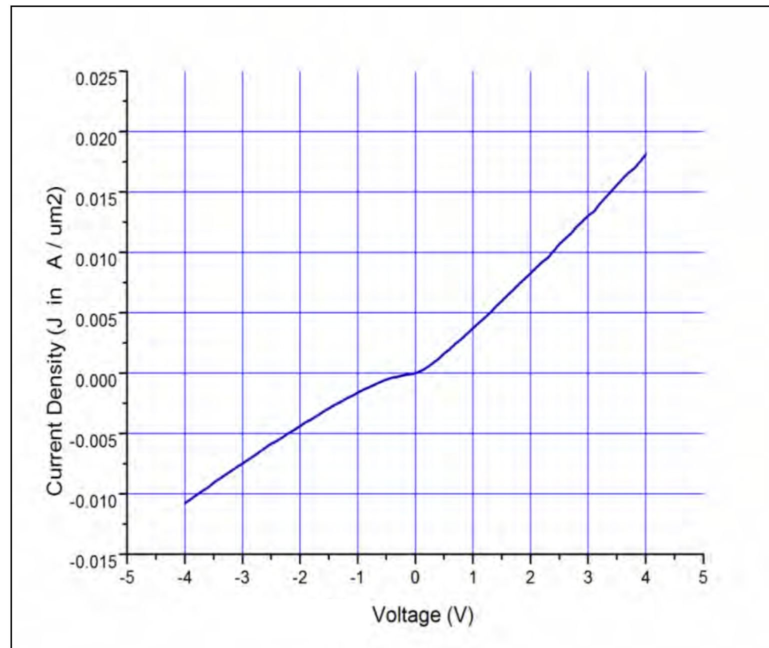

Figure6.1: J-V characteristics curve of p-Si microneedle with a length of 38.57 µm and a diameter of 3.30 µm for a B_2H_6 flow rate of 1.57 sccm.

Table 6.1 : J-V characteristics Data of p-Si microneedle with a length of 38.57 µm and a diameter of 3.30 µm for a B_2H_6 flow rate of 1.57 sccm.

Reversed Bias V_R (Volt)	Current Density J (A/µm^2)	Forward Bias V_F (Volt)	Current Density J (A/µm^2)
-2	-0.19825	0.1	1.8E-05
-1.9	-0.19825	0.2	0.01951
-1.8	-0.17655	0.3	0.06748
-1.7	-0.15705	0.4	0.12938
-1.6	-0.13854	0.5	0.19646
-1.5	-0.12221	0.6	0.26672
-1.4	-0.10709	0.7	0.33639
-1.3	-0.09315	0.8	0.40804
-1.2	-0.08061	0.9	0.47771
-1.1	-0.06927	1	0.54936
-1	-0.05912	1.1	0.61903
-0.9	-0.05056	1.2	0.68869
-0.8	-0.0426	1.3	0.75836
-0.7	-0.03563	1.4	0.82404
-0.6	-0.02946	1.5	0.89371
-0.5	-0.02428	1.6	0.96139
-0.4	-0.01915	1.7	1.02707
-0.3	-0.01499	1.8	1.09475
-0.2	-0.01135	1.9	1.16242
-0.1	-0.00806	2	1.22412

6.3 J-V Analysis

The microneedles were expected to be conductive in both directions. But the Current-voltage (I-V) characteristic of boron doped silicon microneedles was found nonlinear and exhibits rectifying nature (Fig.6.1). The reason behind this rectifying nature is the gold which remains at the top of the needle (Fig .6.2) after the growth. The Au-Si contact at the top of the needle isn't ohmic and the I-V characteristic indicates the presence of Schottky barrier at the top hence metal- semiconductor contact characteristics need to be understood to reveal the fact.

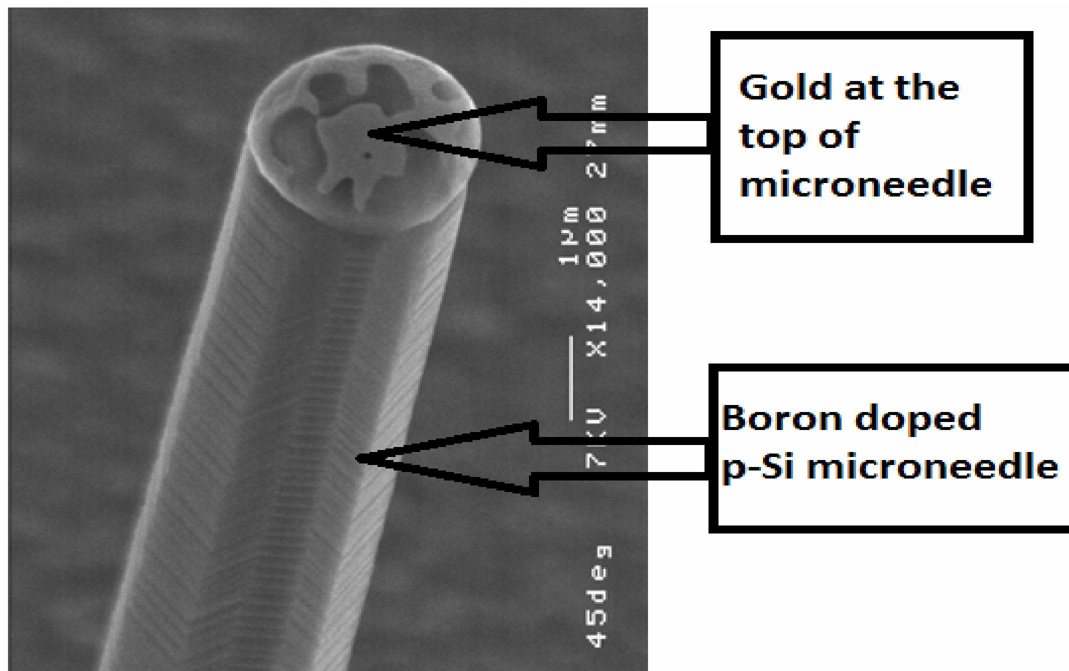

Figure 6.2: SEM image of p-Si microneedle array grown by *in situ* doped VLS [13].

6.3.1 metal-p-type semiconductor contact

If the metal-semiconductor contact is ohmic, charge carriers can flow in either direction without any barrier at the interface. However, actually a potential barrier is always found at the junction. At first Schottky and Mott modeled the barrier formation.

The barrier is mainly due to the difference in the work function of the metal and semiconductor.

In ideal case when gold is brought into contact with the p-type semiconductor, electrons flow from the metal into the empty states in the valence band and hence the bands curve upwards as the chemical potential comes into equilibrium with the metal Fermi level. At equilibrium a region depleted of holes and a potential barrier for holes is formed. The junction is forward biased if the metal is connected to the negative terminal and the holes are attracted towards the interface due to forward biasing (Fig.6.1). In the forward biased condition both the depletion region and the potential barrier is reduced and a large net current flows. In the reversed biased condition i.e. when the metal is connected to the positive terminal the holes are repelled from the interface. The result is increased depletion region and potential barrier and the net current flow is ideally zero.

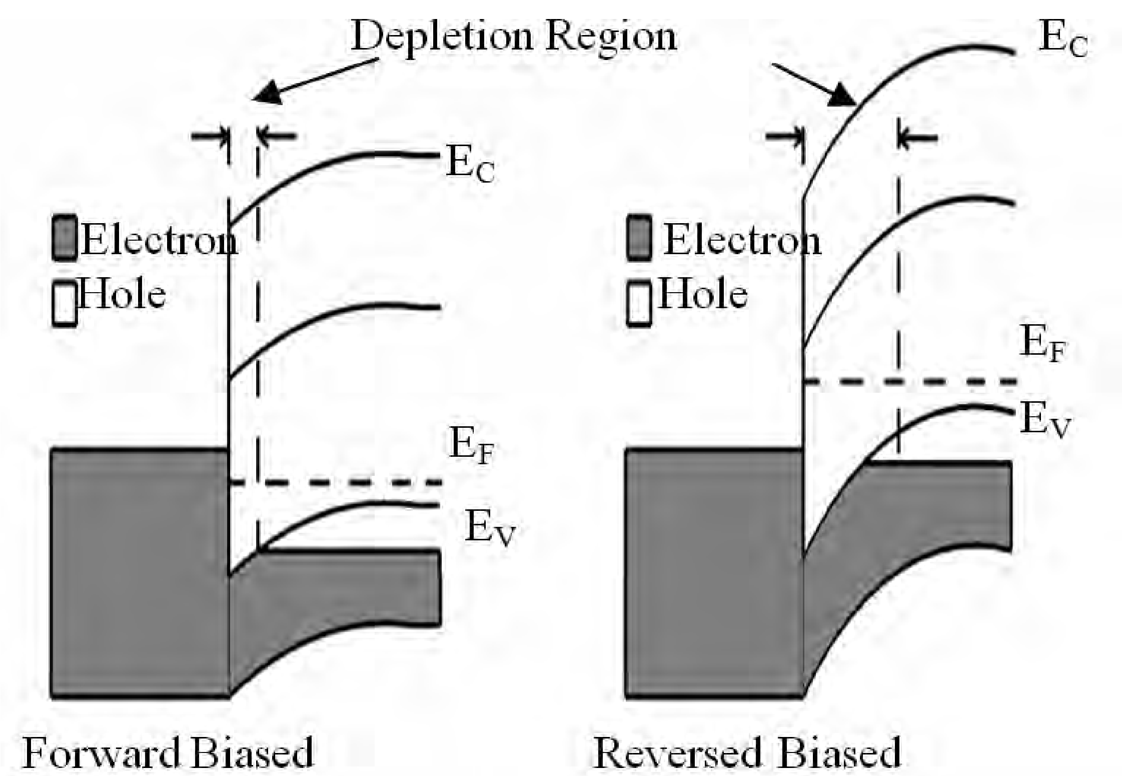

Figure 6.3: Band diagram of Metal-p-Si junction under biased condition.

6.3.2 Simulation Result

A needle shaped boron doped p-Si microneedle with gold at the top as a cathode was simulated for J-V analysis. The length and diameter of the needle was 38.57 um and 3.30 um respectively. The work function of the Au was chosen 5.1 for simulation. At room temperature (300k) with uniformly Boron dopped needle with doping concentration of 3.5×10^{18} cm^{-3} shows almost same J-V characteristics as found experimentally (Fig.6.1). The J-V characteristics curve from simulation is shown in Fig.6.4. The simulation was done for an ideal schottky barrier diode and the doping was chosen to be uniform for simulation.

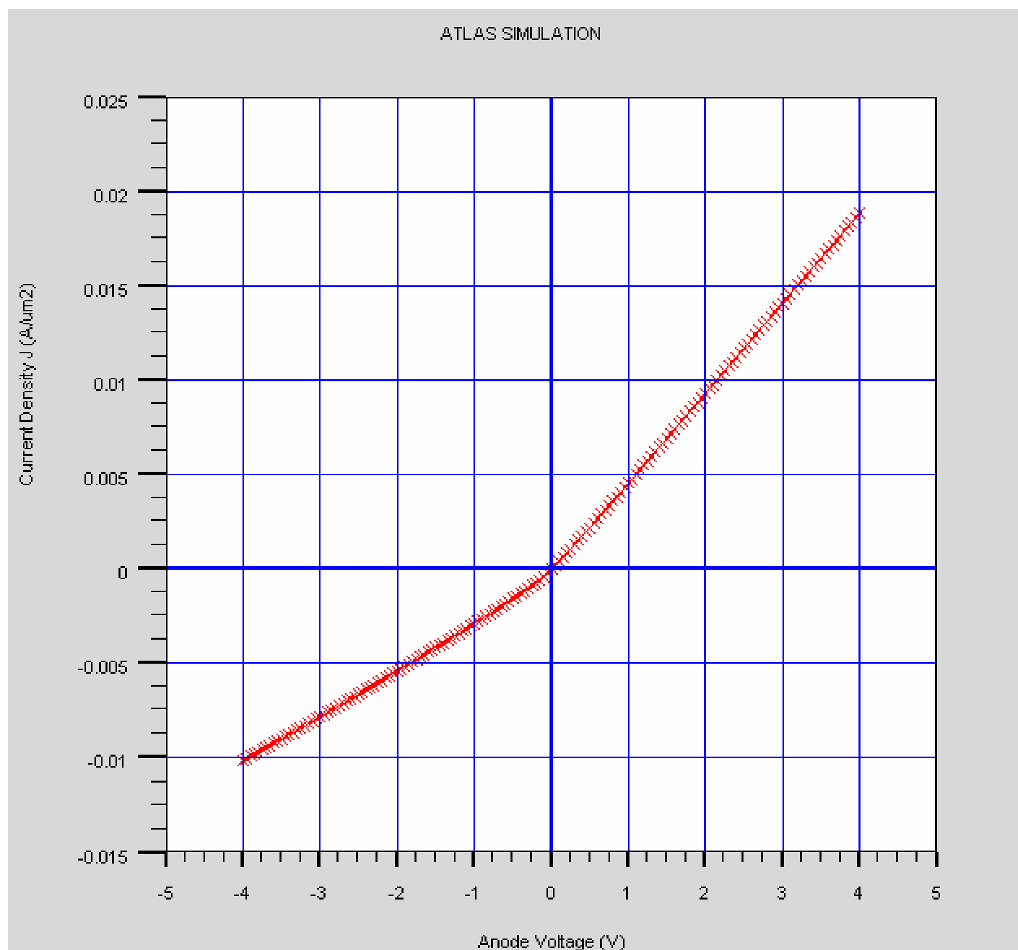

Figure 6.4 : J-V characteristics curve of p-Si microneedle from the Atlas simulator.

6.3.3 J-V Equation

It is obvious that the J-V characteristics, found from the VLS grown boron doped microneedles, indicates towards the fact that the rectifying characteristics is due to the presence of a Schottky barrier at the top. The current transport in Schottky barrier diode is due to mainly majority carrier. The *in-situ* doped VLS grown microneedles are highly conductive and seems to be highly doped as we compared with simulation model. Hence the current transport process is considered to be dominated by quantum mechanical tunneling, thermionic emission process. Tunneling dominates at higher doping and lower temperature. Considering thermionic emission and tunneling, the J-V relationship is given by Sze [30].

$$J = J_0\left[\exp\left(\frac{qV}{\eta kT}\right) - 1\right] \qquad 6.1$$

$$J_o = A^* T^2 \exp\left(-\frac{q\phi_B}{kT}\right) \qquad 6.2$$

Where, J_0 is the saturation current density. $\phi_B = (\phi_{Bo} - \Delta\phi_o)$ is the effective barrier height at zero bias. A* is the effective Richardson constant given by $A^* = (4\pi m^* q k^3/H^3)$. The value of A^* is independent of temperature (Crowell and Sze, 1966) [21]. The effective barrier height at zero bias is given by

$$\phi_B = \frac{kT}{q}\ln\left(\frac{A_d A^* T^2}{I_o}\right) \qquad 6.3$$

Where A_d is the Schottky contact area, I_o is the saturation current at zero bias. The ideality factor η given by

$$\frac{1}{\eta} = \frac{kT}{q}\frac{d}{dV}\ln\left[\frac{J}{\{1-\exp(-qV/kT)\}}\right] \qquad 6.4$$

For V > 3kT/q,

$$\frac{1}{\eta} = \frac{kT}{q} \frac{d(\ln J)}{dV} \quad . \tag{6.5}$$

In the reverse direction the J-V relation is as below

$$J_R \approx A^{**} T^2 \exp\left(- \frac{q(\phi_{B0} - \sqrt{q\xi_m / 4\pi\varepsilon_s})}{kT} \right) \tag{6.6}$$

Where, A^{**} is the modified Richardson constant considering the impact of electron emission and tunneling; ξ_m is the maximum electric field at metal-semiconductor interface and ε_s is the semiconductor permittivity. As no diffused guard ring was introduced during fabrication the sharp edge effect must be present and hence the dominant reverse current is due to the edge leakage. The reverse current must have additional component due to contamination in Au–Si contact as will be discussed later. Due to quantum-mechanical effect some electron from gold penetrates into the silicon energy band and results in a static dipole layer at the Au-Si interface. This dipole layer is responsible for varying barrier height slightly with the field in the reverse bias. The static voltage lowering is expressed as below

$$\Delta\phi_{static} \approx \alpha\xi_m \tag{6.7}$$

6.3.4 Comparison between Experimental and Simulation Result

From the comparison between the simulated and experimental results it is seen that there is some difference between them as shown in Fig.6.5.

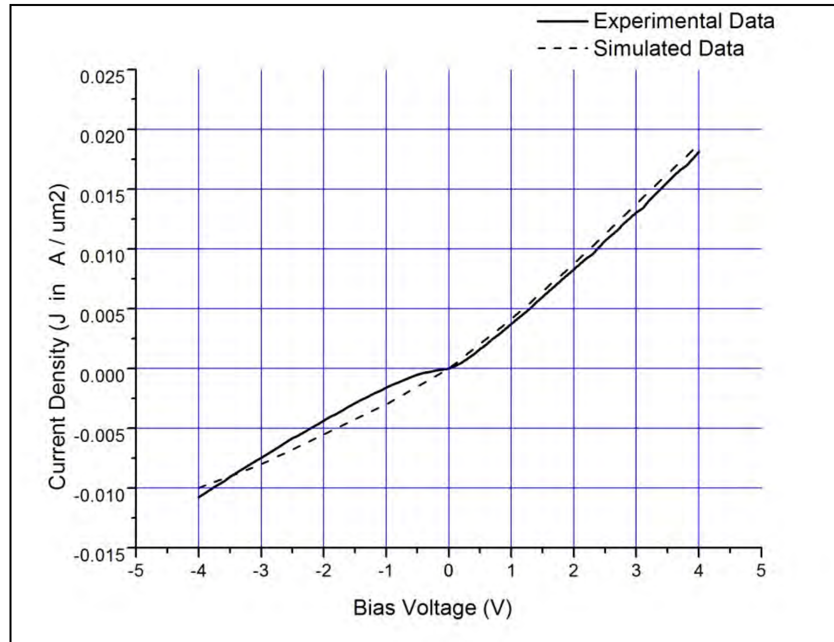

Figure 6.5 : J-V Comparison between the simulated and experimental data

Table 6.2: Table comparing Experimental and Simulated data for J-V characteristic.

Bias Voltage	Experimental Data	Simulated Data
Volt	**J (A/μm^2)**	
-4	-0.01075	-0.01
-3	-0.00746	-0.008
-2	-0.00436	-0.0055
-1	-0.0016	-0.003
0	0	0
1	0.00373	0.00425
2	0.00828	0.00875
3	0.01305	0.01375
4	0.01806	0.01875

This is because for the simulation the needle was assumed uniformly doped. However, in fact the boron may not be uniformly distributed in the VLS grown needles. Again the Current-voltage (I-V) characteristic of boron doped p-Si microneedle was measured by

using tungsten (W) microneedles and hence contact resistance must be present there. It was reported earlier by Ling Pan et al [14] that due to boron doping some gold is lost from the needle tip and mix into the needle during the VLS growth mechanism. Thus the gold at the top is contaminated by Si and gold is also present in the needles. These contaminations must affect the barrier height. The simulation shows that slight deviation in metal work function changes the J-V characteristics particularly in the reverse biased zone (Fig.6.6), the effect is rigorous.

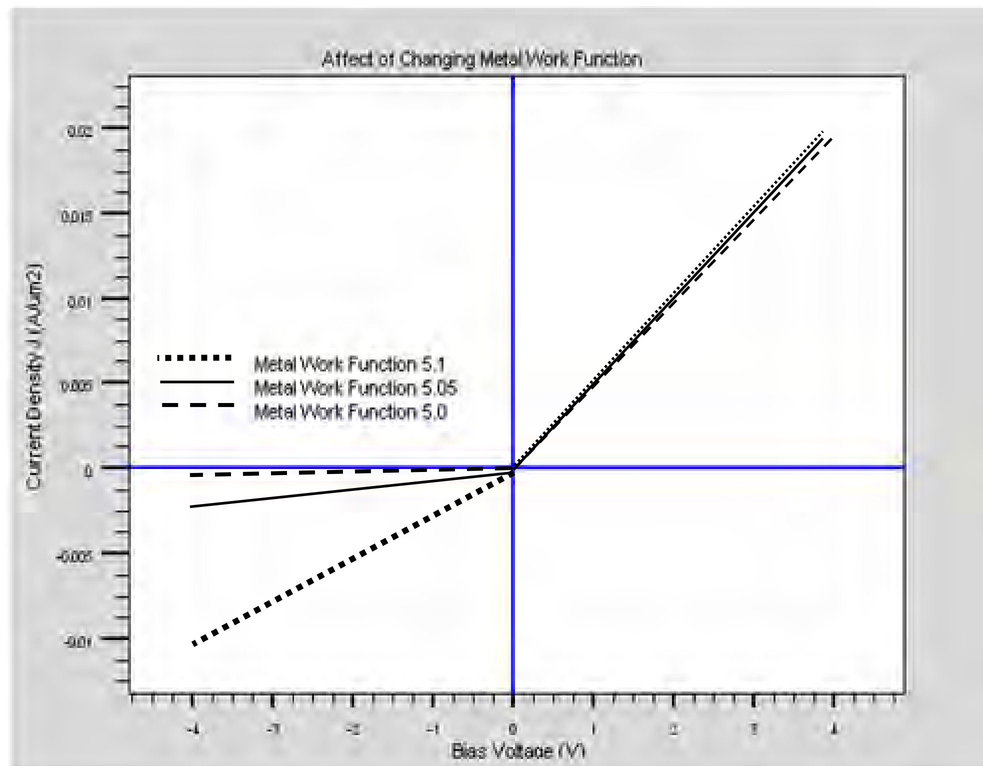

Figure 6.6: Effect of changing work function on J-V characteristics

6.5 Reasons for Deviations from the Ideal Case

Real Schottky diodes do not always follow the expressions or equations. Deviations from ideal behavior arise from imperfections in fabrication or factors. A few of the major factors are given below.

6.5.1. Schottky Barrier Lowering

In ideal case Schottky barrier height remains constant under all conditions of applied voltage. However, practically the barrier height varies with applied voltage because conduction electrons experience a force from their image charges in the metal. This force attracts the electrons toward the metal surface, effectively lowering the barrier, and allowing voltage-dependent deviations from ideal behavior.

6.5.2. Surface Imperfections

The semiconductor surface must be extremely clean in order to realize I/V characteristics approximately the ideal. However, in spite of scrupulous care in fabrication, the junction experiences at least a small amount of contamination due to impurities. The deposition of the junction metal may also damage the crystal structure of the surface.

6.5.3. Tunneling

Thermal emission is not only mechanism by which electrons can cross the potential barrier at the junction. Quantum mechanical tunneling through the barrier is also possible, and may have a significant effect on I/V characteristic at low temperatures and high doping densities.

6.5.4. Series Resistance

Schottky junctions generally require lightly doped semiconductors with relatively high bulk resistivities. A lightly doped substrate would not be practical for diode fabrication because it would result in high series resistance and poor ohmic cathode contacts.

6.5.5 Edge Effects

Practical diodes are formed with a small anode on a large semiconductor surface, so the fringing electric field near the edge of the metal anode is greater than that in the center. The current density is, therefore, greatest at the edge of the junction, and may be relatively low at the center.

CHAPTER 7

Conclusion and Future Work

Chapter 7

Conclusion and Future Works

7.1 Conclusion

A lot of research work has already been done on Vapor Liquid Solid growth of silicon wires or needles, on the synthesis of the wires itself, as well as on their properties. Recently, more specifically for the last decade research into semiconductor whiskers with nanoscale dimensions have become an extremely active field. This can be seen from the vast number of papers (Figure 6.1) published on nanowires over the past two decades, which has increased exponentially, with most of the activity and development happening in the last ten years.

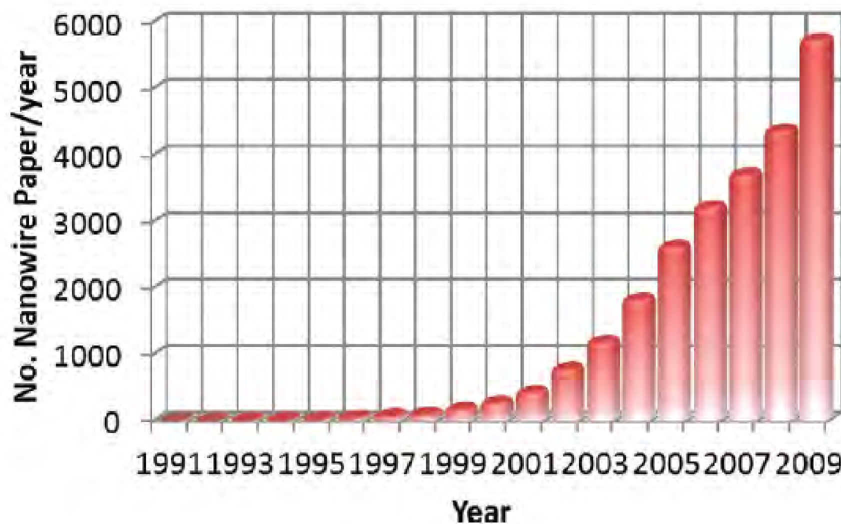

Figure 7.1: Increase in the number of publications on nanowire related topics from year 1991-2009 (Source, ISI; keyword, nanowires).

However, the interest of the researchers in this field exposes the importance of such semiconductor devices. Nevertheless, a number of open questions still remain to be answered. This thesis work has successfully focused on such mystery related to physical and electrical properties of Boron doped Si microneedle grown by *in situ* doped VLS method.

The growth rate and Diameter model and theoretical analysis in this thesis will be very helpful to anticipate the size of such Boron doped microneedles and hence to fabricate microneedles of desired length and width for certain applications.

Moreover, the electrical property of the microneedles and the I-V characteristics is analyzed in chapter 6. The boron doped silicon microneedles grown by VLS mechanism with J-V characteristics like schottky diode can be very useful for a sensor. Therefore, it is vital to obtain a better understanding of the basic electrical properties of the metal-semiconductor interface of the microneedles so that technologies for preparing ideal Schottky contacts at the top of the microneedle can be developed for various applications. The Si micro needles have greater mechanical strength than those of Si nanowires and hence suitable for using as inserting needle to collect small neural signal. Doped Silicon micro needles are more conductive and hence appropriate to collect small signals from living cells. However as doping changes the J-V characteristics of micro needles in VLS mechanism, the complete electrical analysis supported by simulation in this thesis will be very helpful to grow needles of desired characteristics. The detail analysis of the electrical properties of boron doped Si microneedles in this thesis work will also be helpful to improve the J-V characteristics in future while fabricating vertical devices like diodes, transistors with Si microneedles.

7.2 Scope of future research work:

Silicon is utilized in a variety of new commercial products because of its well-established electronic properties but its excellent mechanical property is also used to a great extent. In addition, recent trends in the engineering literature indicate a growing interest in the use of silicon as a mechanical material with the ultimate goal of

developing sensors and transducers. Hence, The Si microneedles have a great prospect to be used as pressure sensors. Some researchers have measured the elastic modulus and hardness of boron-doped silicon material using nano indenter and reported that elastic modulus and hardness of heavy boron-doped silicon material is higher than the silicon material [30]. Therefore, Detail study of the mechanical characteristics of such microneedles is required and there is a huge scope of research in this field.

Optical properties of Si microneedles are already reported by some researchers for use in silicon solar cell applications [32]-[33]. So, it is evident that microneedles can also be realized as photo sensor or photo cell and there is a scope to study the optical properties of such microneedles.

The radial growth dynamics of microneedle due to the vapor solid (VS) process while it grows along its axial direction due to vapor liquid solid (VLS) process was beyond the scope of this thesis work. The experimental result shows that the needles are tapered with a certain slope. Although the slope may be generally very small, it still does exist. The radial growth makes it difficult to grow needles with a uniform radius. Therefore detail study and modeling of the radial growth is utmost important.

Here in this thesis work the effect of changing temperature on the growth rate isn't considered. So, this work also can be extended considering the effect of temperature.

The analysis of electrical properties of boron doped Si microneedles reveals the rectifying nature of the I-V relation which is because of Schottky barrier at the top of the microneedle. By fabricating boron doped silicon microneedles with diffused guard ring more improved needle shaped Schottky diode can be fabricated with less sharp edge effect. Hence there is a scope here to improve the I-V characteristic by modifying the fabrication process.

References

[1]. J.Held, J. Gaspar, P.J. Koester, C. Tautorat, A. Cismak, W. Baumann, A. Trautmann, P. Ruther, and O. Paul, "Microneedle arrays for intracellular recording applications," In: IEEE MEMS congress proceedings, Tucson, USA, pp.268-271, 2008.

[2]. T. Kawano, H. Takao, K. Sawada, and M. Ishida, "Multichannel 5×5-Site 3-dimensional Si microprobe electrode array for neural activity recording system," Jpn. J. Appl. Phys. Vol. 42, pp. 2473-2477, 2003.

[3]. T. Kawano, H. Takao, K. Sawada, and M. Ishida, "Neural recording chip with penetrating Si microprobe electrode array by selective vapor-liquid-solid growth method," IEMBS 2004, pp.2066-2069, September 2004.

[4]. K. Takei, T. Kawashima, T. Kawano, H. Takao, K. Sawada, and M. Ishida, "Integration of out-of-plane silicon dioxide microtubes, silicon microprobes and on-chip NMOSFETs by selective vapor–liquid–solid growth," Journal of micromechanics and micro engineering,Vol.18 ,pp.035033,2008.

[5]. L. Lin and A. P. Pisano, "Silicon-Processed Microneedles," IEEE journal of MEMS, vol. 8, no. 1, March 1999.

[6]. V. Schmidt, H. Riel, S. Senz, S. Karg, W. Riess, U. Gçsele, "Realization of a Silicon Nanowire Vertical Surround-Gate Field-Effect Transistor" Small 2006,Vol. 2, pp. 85-88, 2006.

[7]. A. Ikedo, M. Ishida and T. Kawano, "Out-of-plane high-density piezoresistive silicon microwire/p–n diode array for force- and temperature-sensitive artificial whisker sensors," journal of micromechanics and microengineering, Vol 21, (7pp), 2011

[8]. R. S. Wagner, and W. C. Ellis, "Vapor–liquid-solid mechanism of single crystal growth," Appl. Phys. Lett., vol.4, pp. 89-90, 1964.

[9]. T. Kawano, Y. Kato, M. Futagawa, H. Takao, K. Sawada, and M. Ishida, "Fabrication and properties of ultrasmall Si wire arrays with circuits by vapor-liquid-solid growth," Sensors and Actuators, vol. A 97-98, pp. 709-715, 2002.

[10]. T. Kawano, Y. Kato, R. Tani, H. Takao, K. Sawada, and M. Ishida, "Selective vapor-liquid-solid epitaxial growth of micro-Si probe electrode arrays with on-chip MOSFETs on Si (111) substrate," IEEE Trans. Electron Devices, vol. 51, pp. 415-420, 2004.

[11]. M. S. Islam, T Kawashima, K Sawada, and M.Ishida, "High-yield growth of p-Si microprobe arrays by selective vapor–liquid–solid method using in situ doping and their properties," Journal of Crystal Growth, vol.306, pp.276-282,August 2007.

[12]. K. Hasan, M. S. Islam, “Growth Rate Modeling of Boron Doped Silicon Micro Needle Grown by VLS Mechanism,” ICECE 2010, pp.392-395, December 2010.

[13]. M. S. Islam, K Sawada, and M. Ishida, “VLS growth of doped Si-microprobe arrays using varying PH_3 flow with a fixed flow of Si_2H_6 at low temperature,” ICECE 2008, pp.20-22, December 2008.

[14]. L. Pan, K. K. Lew, J. M. Redwing, and E. C. Dickey, “Effect of diborane on the microstructure of boron-doped silicon nanowires,” Journal of Crystal Growth., vol.277, pp. 428-436, 2005.

[15]. S. B Herner and M. H Clark, “Silicon deposition from BCL_3/SiH_4 mixtures: effect of very high boron concentration on microstructure,” J. Vac. Sci. Tech .B, vol.22, pp.1-5, Jan/Feb 2004.

[16]. S. Wen Hu, Y. Wang, and X. Y. Wang, “Gas Phase Reactions between SiH4 and B2H6,” J. Phys. Chem. A 2003, Vol. 107, pp. 1635-1640, November 2003.

[17]. B. Kalache, P. Roca and A. Fontcuberta , “Observation of Incubation Times in the Nucleation of Silicon Nanowires Obtained by the Vapor–Liquid–Solid Method,” Japanese Journal of Applied Physics, Vol. 45, No. 7, 2006, pp. L190–L193, February 2006.

[18]. B. Ressel, K. C. Prince, and S. Heun, “Wetting of Si surfaces by Au–Si liquid alloys,” J. Appl. Phys, Vol.93, pp. 3886-3892, April 2003.

[19]. Y.V. Naidich, V. Zhuravlev, N. Krasovskaya, “The wettability of silicon carbide by Au–Si alloys,” Materials Science and Engineering A245 (1998) , p.p 293–299, 1998.

[20]. H. Kohno, and S.Takeda, “Periodic instability in growth of chains of crystalline-silicon nanospheres,” Journal of crystal growth, vol.216, pp.185-191, March 2000.

[21]. S. M. Sze, “Physics of Semiconductor Devices” 3rd Edition, John Wiley and Sons, New York, 2007, p. 134-196.

[22]. Yi Cui, Xiangfeng Duan, Jiangtao Hu, and Charles M. Lieber, “Doping and Electrical Transport in Silicon Nanowires,”Journal of physical chemistry, vol.104, pp.5213-5216, June 2000.

[23]. B. Mehta, and M. Tao, “A Kinetic Model for Boron and Phosphorus Doping in Silicon Epitaxy by CVD,” J. Electrochem. Soc., Volume 152, Issue 4, pp. G309-G315, 2005.

[24]. E. I. Givargizov, “Growth of Whiskers by the Vapor-Liquid-Solid Mechanism,” J. Cryst. Growth 1975, Vol. 1, 31, 20, 1975.

[25]. J. Johansson, C.P.T. Svensson, T. Martensson, L. Samuelson, and W. Seifert, “Mass Transport Model for Semiconductor Nanowire Growth,” Journal of physical chemistry, Vol. 109, pp.13567-13571, May 2005.

[26]. H. Schmid, M. T. Bjork, J. Knoch, H. Riel, W. Riess, “Patterned epitaxial vapor-liquid-solid growth of silicon nanowires on Si(111) using silane,” J. Appl. Phys, Vol. 103,pp. 024304-024311,January 2008.

[27]. S. Kodambaka, J. Tersoff, M.C. Reuter, F.M. Ross, “Diameter-Independent Kinetics in the Vapor-Liquid-Solid Growth of Si Nanowires,” Phys. ReV. Lett. Vol. 96, pp. 096105- 096109, March 2006.

[28]. B. Ressel, K.C Prince, S. Heun, Y. Homma, "Wetting of Si surfaces by Au–Si liquid alloys ," J. Appl. Phys, Vol. 93, pp. 3886-3893, January 2003.

[29]. H.Y. Erbil, "Surface Chemistry of Solid and Liquid Interfaces" 1st Edition, Blackwell Publishing Ltd, UK, 2006, pp. 308-337.

[30]. S. M. Sze, "Physics of Semiconductor Devices" 3rd Edition, John Wiley and Sons, New York, 2007, pp. 134-196.

[31]. H. Liu, S. Gao, S. Niu, L.Jin, "Measurements on Mechanical Properties of Boron-doped Silicon Materials for Micro Inertia Sensor," ICEMI'2009, pp. 174-179, October 2009.

[32]. K. Park, Z. Guo,2 H.D. Um, et al , "Optical properties of Si microwires combined with nanoneedles for flexible thin film photovoltaics," Optics Express, Vol. 19, Issue S1, pp. A41-A50 , Janury 2011.

[33]. M. C. Putnam, S. W .Boettcher, et al, "Si microwire-array solar cells," Energy Environ. Sci, Vol. *3*, pp. 1037-1041, August 2010.